


## Polarons in Halide Perovskites: A Perspective

Dibyajyoti Ghosh,<sup>#</sup> Eric Welch,<sup>#</sup> Amanda J. Neukirch, Alex Zakhidov, and Sergei Tretiak\*

 Cite This: *J. Phys. Chem. Lett.* 2020, 11, 3271–3286

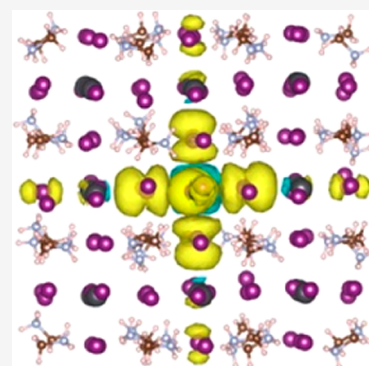
 Read Online

ACCESS |

 Metrics & More

 Article Recommendations

**ABSTRACT:** Metal halide perovskites (MHPs) have rapidly emerged as leading contenders in photovoltaic technology and other optoelectronic applications owing to their outstanding optoelectronic properties. After a decade of intense research, an in-depth understanding of the charge carrier transport in MHPs is still an active topic of debate. In this Perspective, we discuss the current state of the field by summarizing the most extensively studied carrier transport mechanisms, such as electron–phonon scattering limited dynamics, ferroelectric effects, Rashba-type band splitting, and polaronic transport. We further extensively discuss the emerging experimental and computational evidence for dominant polaronic carrier dynamics in MHPs. Focusing on both small and large polarons, we explore the fundamental aspects of their motion through the lattice, protecting the photogenerated charge carriers from the recombination process. Finally, we outline different physical and chemical approaches considered recently to study and exploit the polaron transport in MHPs.



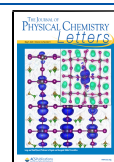
Metal halide perovskites (MHPs) have appeared as one of the most promising materials for a wide range of optoelectronic applications, from solar cells to light-emitting diodes (LEDs) to sensors and radiation detectors.<sup>1–9</sup> Several beneficial characteristics such as a convolution of optimal photophysical properties, inexpensive precursors, and relatively easy room-temperature fabrication have helped these materials to potentially transform modern optoelectronic devices within a decade of time. Particularly, solar cells are at the forefront of MHP research with exceptional device properties like large charge carrier diffusion lengths ( $l = 7.7–10 \mu\text{m}$ ),<sup>10,11</sup> long carrier lifetime ( $t > \mu\text{s}$ ), a strong band-edge absorption coefficient ( $\mu = 1.5 \times 10^5 \text{ cm}^{-1}$ ),<sup>12</sup> low exciton binding energies ( $E_b = 14–41 \text{ meV}$ ),<sup>13,14</sup> optimal bandgaps ( $E_g = 0.5–5.0 \text{ eV}$ ),<sup>15,12</sup> and high defect tolerance.<sup>16,17</sup> These attractive properties coupled with an abundance of low-cost device component options explain intense research efforts that have resulted in the greater than 24% power conversion efficiency, up more than 10% in just 5 years.<sup>18</sup> Along with solar cells, MHPs have also provided extensive opportunity to strategically design a wide variety of LEDs, with high color purity to high color rendition.<sup>19–22</sup> Strongly bound excitons and their interaction with lattice and point defects result in very different and highly tunable emissive properties for layered MHPs.<sup>23,24</sup> The photodetectors made of MHPs have shown fast photoresponse and large detectability at room temperature, largely compatible with commercial Si photodetectors.<sup>5,25–27</sup> Moreover, MHPs have been used for high-energy radiation detectors because of properties such as their ability to interact with high-energy photons and low leakage current under high electric fields.<sup>28–30</sup>

While MHP materials offer a promising alternative to more expensive semiconductor-based devices, long-term structural stability remains the one crucial hurdle to overcome by MHP devices.<sup>31,32</sup> Most photoactive three-dimensional (3D) halide perovskites degrade upon being exposed to oxygen, moisture, heat, mechanical stress, reverse bias, and even under light illumination, strongly affecting their device performance.<sup>33–36</sup> Several approaches like extensive compositional engineering, application of the resistant coating, and replacement of metal electrodes are found to be effective at increasing the stability of these devices.<sup>37–40</sup> Another more intrinsic and fundamental issue that limits the strategic development of MHP-based photovoltaic devices is the understanding and optimization of charge carrier dynamics in these materials.<sup>16,41–47</sup> The community has witnessed a constructive debate over the dominating processes of carrier transport from the beginning of the MHP-related research. In this Perspective, after a brief discussion on the structure of MHPs, we summarize most of the well-explored carrier transport mechanisms for these materials.<sup>10,47–57,44,58–64</sup> We further focus on the polaronic behavior of carriers in MHPs. The concept of polarons has been used to explain multiple photophysical phenomena in these materials, and their presence has demonstrated both beneficial as well as detrimental effects.<sup>52,57,65–70</sup> A robust understanding of electron–phonon interactions and the

**Received:** January 2, 2020

**Accepted:** March 27, 2020

**Published:** March 27, 2020



## A robust understanding of electron–phonon interactions and the transport of polarons remains crucial to bringing MHP active-layer materials beyond lab-scale and into the consumer market.

transport of polarons remains crucial to bringing MHP active-layer materials beyond lab-scale and into the consumer market. Because of the vastness of the field, in this Perspective, we concentrate on the effects of polarons in 3D halide perovskites only. We further refer an interested reader to the recent Perspective on polarons in two-dimensional MHPs.<sup>71</sup>

**Structure of Halide Perovskites.** Perovskite compounds, such as the mineral  $\text{CaTiO}_3$ , form an  $\text{ABX}_3$  structure, where A is a large mono- or divalent cation, B a multivalent cation usually smaller than A, and X an anion. The ideal  $\text{ABX}_3$  structure has a 6-fold coordinated B atom forming  $\text{BX}_6$  octahedra surrounding 12-fold coordinated A cations<sup>72</sup> (see Figure 1a); while this

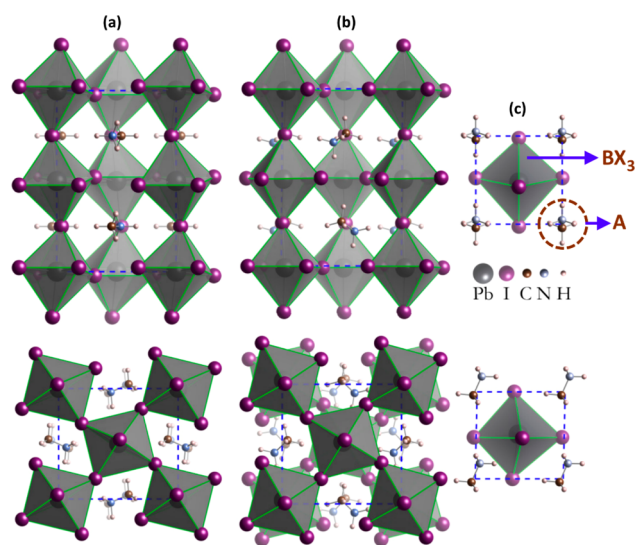


**Figure 1.** Crystal structures of the (a) orthorhombic, (b) tetragonal, and (c) cubic phases of  $\text{MAPbI}_3$  (MAPI, MA =  $\text{CH}_3\text{NH}_3$ ) halide perovskite. The upper and lower panels are oriented through  $\langle 100 \rangle$  and  $\langle 001 \rangle$  planes, respectively. The gray octahedron represents  $\text{BX}_3$ .<sup>80</sup> Reproduced from ref 80. Copyright 2015 American Physical Society.

cubic structure is ideal, perovskites may also be rhombohedral, orthorhombic, or tetragonal or form lower-dimensional structures as well (see Figure 1 for some examples). A, B, and X are often chosen based on the Goldschmidt tolerance factor which quantifies the ratio of the constituent atomic radii (i.e.,  $r_A$ ,  $r_B$ , and  $r_X$ ) that will form a perovskite structure given by<sup>73</sup>

$$t = \frac{r_A + r_X}{\sqrt{2}(r_B + r_X)} \quad (1)$$

where  $t$  values from 0.9 to 1.1 are usually considered the range in which crystals stabilize in the perovskite structure. Octahedral distortions due to slightly larger or smaller A or B atoms may still result in the perovskite structure with values above and below 0.9 and 1.1, respectively. This implies that the tolerance factor is only a first approximation to predicting a

perovskite structure. When halide atoms fill the X site, A and B must have a combined formal charge of +3 to ensure overall charge neutrality in the compound, with the most common halides of interest in MHP-active layer materials being I, Br, and Cl. Inorganic halide perovskite often utilize group I or II atoms like Cs at the A site along with metals like Pb at the B site to form a perovskite structure. A subset of MHPs, hybrid organic–inorganic halide perovskites utilize organic molecules like methylammonium (MA) or formamidinium (FA) at the A site along with metals like Pb or Sn at the B site.<sup>42</sup> To account for the deviated shapes of the molecular A-cations from the ideal sphere, the revised Goldschmidt tolerance factor has been proposed where the molecular globularity replaces the ionic radii of A-cations.<sup>74</sup> Moreover, MHPs employ a variety of stoichiometric ratios. For example, a general formula  $\text{MA}_{1-x-y}\text{FA}_x\text{Cs}_y\text{Pb}_{1-n}\text{Sn}_n\text{I}_{3-m-p}\text{Br}_m\text{Cl}_p$  refers to a combination of Cs, MA, and FA at the A sites, Pb and Sn at the B sites, and Br and I at the X sites, where  $x$ ,  $y$ , and  $n$  range from 0 to 1 and  $m$  ranges from 0 to 3.<sup>37,75–79</sup> This complex perovskite structure, while resulting in the most efficient solar cell device to date, still remains a computational and engineering challenge when attempting to rationalize and predict the correct stoichiometric values.

**Phases of Halide Perovskites.** Numerous perovskite phases exist which satisfy the requisite geometry and reside within 0.1 of the ideal Goldschmidt factor range. However, three primary phases correspond to cubic, tetragonal, and orthorhombic structures, as shown in Figure 1.<sup>80</sup> Typically, a low-temperature phase transition appears from an orthorhombic to a tetragonal structure, while a high-temperature phase change occurs from a tetragonal to a cubic structure. Considering  $\text{CH}_3\text{NH}_3\text{PbI}_3$  (MAPI) as an example, the orthorhombic phase ( $Pnma$ ) changes to the body-centered tetragonal phase ( $I4/mcm$ ) around 160 K, and the tetragonal phase transforms to the cubic phase ( $Pm\bar{3}m$ ) at 330 K.<sup>81</sup> All these phase transitions are found to be first-order transitions. During these phase transitions, the most dominant structural change is the rigid rotation of the  $\text{PbI}_6$  octahedra. In the high-temperature cubic  $Pm\bar{3}m$  structure, the octahedra have high symmetry and do not exhibit any rotations.<sup>81</sup> However, in both low-temperature phases, octahedra rotate and induce low symmetries. Along with inorganic octahedra, phase transitions distinctly affect the organic cation dynamics in MHPs.<sup>80,82,83</sup> In the orthorhombic phase, orientations of A cations remain fixed toward an open face of the inorganic cube. With an increase in temperature, the A-cation dynamics get activated at the tetragonal phase, and these cations become rotationally disordered in the structure. In the high-temperature cubic phase, the extent of the disorder increases for A-cations where they perform almost barrier-free rotation and tumbling inside the inorganic framework. As discussed later, these phase transitions and the associated changes in structural dynamics strongly affect the atomistic mechanisms of charge carrier dynamics and transport in MHPs.

**Charge Carrier Transport in Halide Perovskites.** The exact mechanism of the charge carrier dynamics in MHPs has been investigated by several experimental techniques and a variety of computational methods. In the following section, we summarize a few reported important aspects for carrier dynamics in these materials such as electron–phonon interactions, ferroelectricity, Rashba–Dresselhaus splitting of band-edges, and polaronic effects.

1. *Dynamic Interactions between Charge Carriers and Crystal Vibrations.* Because of the softness of halide perovskites (typical reported hardness for MHP is <1 GPa), lattice vibrations are believed to have substantial effects on charge carrier dynamics through the electron–phonon coupling.<sup>48,56,84,85</sup> For example, carrier mobility increases with decreasing temperature in halide perovskites, indicating a strong relevance of phonon modes to the carrier transport.<sup>86</sup> The electron–phonon interactions also participate in hot carrier relaxation, the process by which charge carriers transfer their extra energy to the lattice.<sup>87,88</sup> Moreover, unique dielectric response of MHP suggests pronounced charge–lattice dynamics. Figure 2 shows the range of frequency-

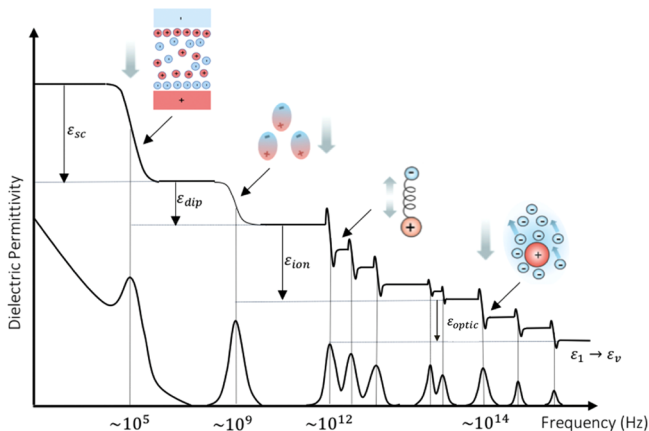


**Figure 2.** Frequency-dependent dielectric spectrum for MAPbI<sub>3</sub>. The top line is the real and the bottom line (peaks) is the imaginary part of the dielectric function. The images imposed over the top line show the physical mechanisms which contribute to each resonance region. Reproduced from ref 89. Copyright 2019 APL Materials.

dependent dielectric values for MAPbI<sub>3</sub> (up to petahertz), where the static ( $\epsilon_r(0)$ ) dielectric constant is much larger than the optical ( $\epsilon_r(\infty)$ ) dielectric constant;<sup>89</sup> the superimposed images indicate the physical processes that result in the dielectric response at a given frequency in typical MHPs.

Broadly, two mechanisms have been put forward to understand the interaction between charge carriers and lattice vibrations: (1) acoustic deformation potential scattering<sup>56,90–92,84</sup> and (2) Fröhlich type polar interactions.<sup>47–49</sup> In deformation potential scattering, crystal vibrations displace the atoms from their lattice sites, inducing temporary structural distortions. These distortions modify the electronic band structure of the material, eventually resulting in the coupling of the electrons with acoustic phonons. In contrast, for polar interactions, the polarization of the ionic lattices imposes electric fields and that couples to electrons of the system. Mostly, longitudinal optical (LO) phonon modes create a macroscopic electric field through Fröhlich interactions, producing the polarization.<sup>93,94</sup>

The strong influence of the deformation potential scattering on the carrier mobility of MHPs has been studied recently. Karakus et al.<sup>95</sup> have performed ultra-broadband time-resolved terahertz (THz) spectroscopy measurements on the MAPI thin films, proposing a simple Drude-like model to explain the temperature dependence of the carrier momentum scattering times and carrier mobilities. In the Drude model,<sup>96</sup> the carrier-mobility ( $\mu$ ) depends on two factors, the effective mass of the

electron ( $m_e^*$ ) or the hole ( $m_h^*$ ) and the carrier momentum relaxation time ( $\tau$ ), by the relation

$$\mu = e\tau/m^* \quad (2)$$

Thus, in a system where effective masses do not change with temperature, the carrier scattering time dominantly influences the carrier mobility. In this study,<sup>95</sup> the authors found a power-law relation between the charge-carrier scattering times ( $\tau$ ) and temperature ( $T$ ) for tetragonal MAPI,  $\tau \propto T^{-3/2}$  (see Figure 3a).<sup>86,95</sup> This kind of a power-law relation is characteristic of the system where free carrier transport is limited by the deformation potential scattering. Thus, acoustic phonon–electron scattering is the dominant factor influencing the charge carrier mobility in MAPI at the room-temperature phase. Using density functional theory (DFT)-based computations, Zhao et al. have further calculated the deformation potential for electrons and holes in tetragonal and cubic phases of MAPI.<sup>56</sup> By applying semiclassical Boltzmann transport theory in the relaxation time approximation, this study reported high carrier mobilities in the range for few hundreds to few thousands of  $\text{cm}^2 \text{V}^{-1} \text{s}^{-1}$  (see Figure 3b). These high mobility values are attributed to a weak charge–acoustic phonon scattering. This study further demonstrated that the inclusion of carrier scattering via Coulomb interactions with charged impurities or defects can significantly reduce the mobility values in MAPI. Considering impurity density as  $10^{18} \text{ cm}^{-3}$ , at 300 K the carrier mobilities were calculated to be in the range of  $72\text{--}178 \text{ cm}^2 \text{V}^{-1} \text{s}^{-1}$  in agreement with the experimental reports.<sup>47,48</sup> Thus, this study concluded that impurity-scattering can be a dominating mechanism for charge carrier dynamics in MHPs.

Group theory analyses were also used for exploring electron–phonon coupling in the weak coupling regime, where independent particle approximation remains valid.<sup>97,98</sup>

It has been shown that with a first-order acoustic deformation potential (ADP), the acoustic phonons get involved in intervalley nonpolar deformation couplings between the frontier bands in the cubic phase of MHPs. Additionally, the dominant effect of spin–orbit coupling at the conduction band minima is expected to couple to local volumetric strain at the conduction band minima (CBM) and valence band maxima (VBM) states.

In addition to impurities as discussed above, recent experimental and computational studies have pointed out that polar LO phonon–electron coupling, i.e., the Fröhlich interaction, also strongly affects the charge carrier dynamics in the halide perovskites at room temperature.<sup>47–49,94</sup> According to this mechanism, the LO phonon modes scatter the charge carriers and thus limit their mobility in solids. A detailed computational study has shown that three distinct low-frequency (below 22 meV) LO vibrations, namely, the Pb–I–Pb bending, the A-cation displacement, and the Pb–I stretching modes, contribute to the electron-scattering rate of lead iodide perovskites via Fröhlich interaction (see Figure 3c–e).<sup>94</sup> The relative contributions of these modes (Figure 3c,e) further demonstrate that the Pb–I stretching is the primary mode for scattering the charge carriers. Based on this mechanism, the upper limits to the charge-carrier mobilities have also been calculated from the values of the LO phonon mode energies and dielectric functions. For MAPI, calculated maximum average carrier mobility, i.e.,  $80 \text{ cm}^2 \text{V}^{-1} \text{s}^{-1}$ , is close to the reported experimental value,  $67 \text{ cm}^2 \text{V}^{-1} \text{s}^{-1}$ , with single crystals. This indicates that high-quality hybrid perovskite



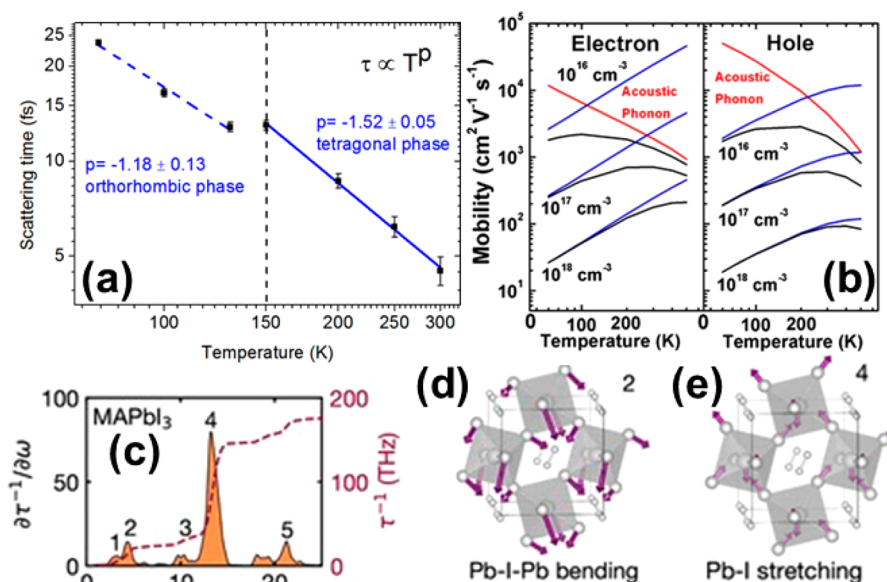


**Figure 3.** (a) Scattering times versus temperature for a MAPbI<sub>3</sub>(Cl) perovskite film sample derived from ultrabroadband terahertz (THz) photoconductivity measurements. Reproduced from ref 95. Copyright 2015 American Chemical Society. The exponent value for the power-law relation approaches 3/2 for a room-temperature phase. However, the smaller exponent value for the low-temperature orthorhombic phase suggests the presence of impurity scattering at low *T*. (b) Temperature dependence of the charge carrier mobility in tetragonal MAPI in the [001] direction calculated using DFT and semiclassical Boltzmann transport theory. Reproduced from ref 56. Copyright 2016 Nature Research. The free carrier density was considered as 10<sup>14</sup> cm<sup>-3</sup>, and the charged impurity density varied as shown in the plot. The black, red, and blue lines represent the total mobility and that limited by acoustic phonon and charged impurity scatterings, respectively. (c) Spectral decomposition of the contribution of each phonon mode to the electron scattering rate in MAPI at 300 K, calculated using *ab initio* many-body computational simulations. Reproduced from ref 57. Copyright 2019 American Chemical Society. The height of the peaks designates the involvement of each phonon mode (left vertical axis), and the integral  $\int (\partial\tau^{-1}/\partial\omega) d\omega$  produces the total scattering rate (right vertical axis).<sup>57</sup> The LO phonon modes corresponding to peaks 2 and 4 in panel c are provided in panels d and e.

crystals are reaching the intrinsic theoretical limit for the carrier mobility. Moreover, the character of these LO phonon modes and their interactions with charge carriers remain mostly unaffected with the variation of A-cations in halide perovskites.<sup>94</sup> Comparing the phonon spectra for CsPbI<sub>3</sub> and MAPbI<sub>3</sub>, one finds that the presence of organic A-cations just broadens the LO phonon peaks because of vibrational coupling between the PbI-cage and MA cations. Thus, at the atomistic level, the charge carrier transport mechanism is identical for inorganic and hybrid halide perovskites.

Considering the Fröhlich interaction as the most influential factor, the effect of compositional engineering on carrier mobility has been widely explored. It has been demonstrated that as Pb atoms get replaced by a lighter B atom, e.g., Sn, the LO phonon frequencies increase, causing an enhancement in the carrier mobility at room temperature.<sup>99</sup> The substitution of I with lighter Br in MAPbX<sub>3</sub> also leads to a higher mobility for Br-based perovskites.<sup>48,100</sup> However, as the ionicity of the Pb–X bond increases from I to Br to Cl, it has been argued that the Fröhlich interactions increase and mobility decreases with lighter halogen-based perovskites.<sup>94,100</sup> Thus, resolution of the exact dependence of mobility with halogen substitution needs more accurate experimental probes and more complete computational models. Nonetheless, these insights are extremely valuable for designing halide perovskites with high-carrier mobility for various applications.

**2. Ferroelectricity.** Ferroelectric materials possess reversible spontaneous polarization below a critical temperature, called the Curie temperature (*T<sub>C</sub>*), above which the transition from an ordered to a disordered phase is triggered.<sup>93,101,102</sup> Ferroelectric materials are noncentrosymmetric polar dielectric

crystals in which an applied electric field can switch the polarization between two or more stable directions. Regarding the microscopic origin of ferroelectricity, there are two mechanisms: (1) low-temperature ordering of a disordered structure in which the resulting structure has directed permanent dipoles and (2) the cooperative motion of ions leading to the incorporation of directed finite dipoles below *T<sub>C</sub>*. For perovskite oxides, like PbTiO<sub>3</sub> and BaTiO<sub>3</sub>, Ti atoms move from the center of BO<sub>3</sub> (B = Pb/Ba) at low temperatures, causing a macroscopic polarization in the system.<sup>102</sup> Moreover, the presence of stereoselective lone pair in B-sites can also induce polar distortion by moving A-site cations, as happens in BiFeO<sub>3</sub>.

For Pb-based MHPs, the lone pair driven ferroelectricity was proposed initially; however, the experimental confirmation of that is yet to be reported.<sup>103</sup> Most studies investigating polarization in MHPs pointed to the dipolar organic A-cations (e.g., MA cations) being the source of ferroelectricity.<sup>51,52,54</sup> These organic polar cations, which are able to rotate inside the cuboctahedral cage of Pb/X at room temperature, freeze to particular orientations at low temperatures. For MAPbI<sub>3</sub>, as tetragonal to orthorhombic phase transition happens at ~160 K, the MA cations freeze to form antiferroelectric ordering, where dipoles orient in opposite directions in alternating lines (see Figure 4a).<sup>80</sup> However, the existence of the ferroelectric phase at room temperature and its effects on the MHP-based solar cell devices have been debated in the literature.<sup>104</sup>

The presence of the ferroelectric phase at operating conditions was argued to be advantageous for MHP photovoltaics: As discussed by Frost et al., the strong lattice polarization can efficiently separate photogenerated charges

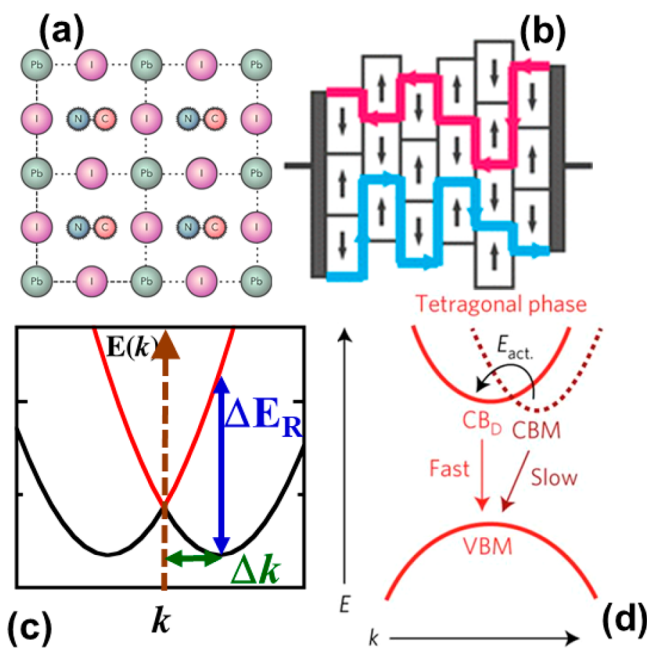


**Figure 4.** (a) Schematic of the MAPI crystal structure with the ferroelectric ordering of MA cations. (b) Schematic for multidomains of ferroelectric MAPI thin films. Reproduced from ref 105. Copyright 2014 American Chemical Society. The transport pathways for holes and electrons are represented by red and blue bold solid lines, respectively. These pathways are called the “ferroelectric highways” for charge transport. (c) Spin-splitting of the conduction band and associated parameters as discussed in the text. (d) Schematics of charge recombination pathways in spin-split bands containing MHPs. Reproduced from ref 107. Copyright 2017 Nature Research. The indirect bandgap proposed hinders the electron–hole recombination and increases carrier lifetime.

enhancing the carrier lifetime and even increase the open-circuit voltages of MHPs above the bandgap.<sup>105</sup> In the proposed mechanism, the built-in electric field in the ferroelectric domains efficiently separates the photogenerated excitons, similar to a traditional p–n heterojunction. As the size of these ferroelectric domains is on the nanometer scale, the probability of recombination of separated charges reduces significantly. As these protected carriers diffuse to the ferroelectric domain boundaries, the same type of carriers accumulate in a particular region as determined by the local dipole-induced electric potential.<sup>105</sup> Following that, the accumulated carriers diffuse toward collecting electrodes along the “ferroelectric highways” without encountering opposite types of charges as shown in Figure 4b. Such spatial separation of electrons and holes inside the material and their quick transport through the ferroelectric domain surface have been argued as the fundamental reason for a long carrier diffusion length in MHPs.<sup>105</sup>

A recent study by Garten et al. reported piezoelectric measurements and several modern scanning probe techniques to confirm the ferroelectricity of MAPI at room temperature.<sup>106</sup> Using electrostatic force microscopy, this study also showed the domain-specific electrical response in MAPI, implying that ferroelectric-induced field can be engineered into working devices to facilitate the photovoltaics of MHPs.

**3. Rashba–Dresselhaus Interaction.** Most of the high-performing MHPs have heavy elements in the structure, such as lead, tin, and iodine.<sup>42</sup> Because of the high atomic number

of these, MHPs exhibit large spin–orbit coupling (SOC) that may impose giant splitting in the band edges.<sup>44,59,61,63,64</sup> The presence of strong SOC substantially affects the optoelectronic properties such as bandgap, alignment of band edges, the carrier effective masses, and the oscillator strength of the optical transitions across the bandgap.<sup>35,59,108</sup> Moreover, the absence of local or extended inversion symmetry in MHPs lattices has been argued to incorporate Rashba and/or Dresselhaus couplings, lifting the 2-fold degeneracy of frontier bands in these materials.<sup>44,59,61</sup> Lattices with site inversion asymmetry causes the Rashba effect,<sup>109</sup> whereas bulk inversion asymmetry results in the Dresselhaus effect.<sup>110</sup> The strength of both effects can be linked to the parameter

$$\alpha = E_R/2\Delta k \quad (3)$$

where  $E_R$  is the amplitude of the spin-splitting in a particular  $k$ -direction and  $\Delta k$  is the momentum offset, i.e., the difference between the  $\Gamma$ -point and shifted band-extrema along the  $k$ -path (see Figure 4c).<sup>59,62</sup> Various computational approaches based on DFT and GW approximations have been extensively used to calculate the  $\alpha$  values as well as in-plane spin texture for static and dynamic structures of different MHPs.<sup>40,76,111–113</sup> Experimentally, spin-dependent circularly polarized pump–probe techniques have been used to identify the spin-splitting and a spin lifetime of the carriers in MAPI.<sup>114</sup> Later, Niesner et al. used angle-resolved photoelectron spectroscopy in MAPbBr<sub>3</sub> single-crystals and demonstrated spin-splitting of the VBM with large Rashba parameters of  $7 \pm 1$  and  $11 \pm 4$  eV Å for orthorhombic and the cubic phase, respectively.<sup>63</sup> Extensive studies show that several factors, such as dynamical fluctuations, A-cation mixing, and the presence of compressive strain, can impose structural symmetry breaking in these soft MHP lattices, resulting in Rashba and/or Dresselhaus effects.<sup>40,76,62</sup>

To explore the effects of spin-splitting on charge carrier dynamics in MAPI, Zheng et al. combined first-principles calculations and a Rashba spin–orbit model.<sup>61</sup> This study demonstrated that SOC-induced Rashba splitting gives rise to spin-allowed and spin-forbidden recombination channels with very different carrier recombination rates. The mismatch of spin and momentum makes the rate significantly slower in the spin-forbidden path (see Figure 4d). Even though the spin-allowed recombination path has a faster rate, this relaxation can be blocked with a suitable spin texture where the fast carrier relaxation to the band edges causes a low concentration of free carriers. Thus, the dominance of spin-forbidden transitions at the band edges has been proposed as the intrinsic reason for a long carrier lifetime in these MHPs.<sup>61</sup> Furthermore, Yu has shown that the giant Rashba effect significantly enhances acoustic-phonon scattering (APS) at low temperature (<100 K), altering the temperature dependence of carrier mobility in MAPI.<sup>44</sup>

Experimentally, with temperature-dependent time-resolved photoluminescence and microwave conductance measurements, Hutter et al. have demonstrated a direct–indirect bandgap character in MAPI.<sup>107</sup> The second-order band-to-band carrier recombination of photoexcited charges was found to be a thermally activated process where slow phonon-assisted recombination occurs via the indirect bandgap. The SOC-induced spin-splitting of band edges has been argued as the origin of this indirect bandgap.<sup>107</sup>

Application of hydrostatic pressure to induce structural distortions has also been proposed to stabilize the Rashba-type

effects and consequently form indirect bandgap in MHPs.<sup>40</sup> Recent experimental results validated this approach by showing pronounced effects of strain on charge carrier dynamics.<sup>58</sup> In this experimental work, the authors found a substantial enhancement of photoluminescence (PL) lifetime under compressive strain, which increases the Rashba effect through SOC in the material.

A common growing consensus in the field is that lattice interactions lead to the formation of polarons and that the carrier transport can be rationalized as polaron dynamics in MHPs.

**4. Polarons.** The above discussion has outlined possible mechanisms of lattice interactions affecting carrier dynamics in MHPs. A common growing consensus in the field is that these interactions lead to the formation of polarons and that the carrier transport can be rationalized as polaron dynamics in MHPs.<sup>70,85,100,115,116</sup> This concept has been widely explored by both experimental tools and computational simulations to rationalize and optimize the charge carrier dynamics in these materials.<sup>117,118</sup> In a solid, electronic carrier interaction with surrounding atoms forms a distortion in the local bonding environment, leading to its spatial localization and confinement.<sup>121</sup> Such a composite of an electronic carrier and a concomitant distorted local lattice constitute a notion of a polaron, one of the most commonly formed quasiparticles in highly polarizable solids.<sup>117,119</sup> Depending on the extent of spatial localization of the carriers, mostly two types of polarons (large and small polarons) can be distinguished.<sup>121</sup> For large polarons, the carriers are distributed over multiple lattice sites, whereas small polarons are formed by the charges localized over a single or few bond lengths. In the following section, we provide a brief overview of polaron physics and then discuss possible features of polaron dynamics in MHPs.

**Basics of Polaron Transport.** A polaron's motion through a crystal lattice is classified as either coherent or incoherent transport.<sup>120</sup> Coherent transport occurs when a carrier moves through a medium with minimal scattering events and mobility being greater than  $1 \text{ cm}^2 \text{ V}^{-1} \text{ s}^{-1}$ .<sup>117</sup> Large mobility, however, does not necessarily indicate a large velocity, as the mobility for coherent transport is momentum-dependent and represents instead a large effective mass. This means coherent transport is usually indicative of large polarons that move with low velocities but have large momenta due to their large effective masses.<sup>121</sup> The mean-free-path between scattering events for coherent transport of a polaron is usually larger than its size except for the case when localization is disrupted by the length of the mean-free-path.<sup>117</sup> Boltzmann's transport equation for mobility may be used to evaluate the minimum mobility for coherent transport when the mean-free-path length is replaced with the polaron's diameter.<sup>118</sup> Incoherent transport, on the other hand, occurs as phonon-assisted hops between lattice sites with mobility much less than  $1 \text{ cm}^2 \text{ V}^{-1} \text{ s}^{-1}$ . Small mobility does not necessarily mean a low velocity, as the effective mass for polarons moving incoherently is typically small. Thus, incoherent transport is usually indicative of a small polaron as sufficient scattering events localize the carrier, where the mean-free-path between collisions is smaller than

the polaron's diameter.<sup>117</sup> While delocalized mobile carriers usually move coherently through minimal scattering events as large polarons, an initially delocalized eigenstate may, through enough scattering events, become localized and lose coherence. This indicates that accurate polaron transport models require the knowledge of both the size of a polaron (i.e., a measure of its localization) as well as its scattering dynamics (i.e., a measure of its coherence), as instances may exist where a large polaron moves incoherently or vice versa, e.g., via Wannier–Stark eigenstates.<sup>118</sup>

**Polarons in Semiconductors.** Polarons were first described by Landau<sup>119</sup> as electronic charge carriers moving slowly through a crystal lattice along with an accompanying motion of the atoms surrounding the mobile charge carrier. These shifted ions then create a potential well around the carrier. If the carrier remains stationary within the well for an extended period of time, it is defined as a self-trapped carrier. A polaron can still form, however, even if it is not self-trapped, as the charge carrier still displaces the ions around it, creating a phonon-cloud of distortion. The range of the interaction of the charge carrier with the phonons of the surrounding lattice is then quantified by the distance over which the interaction occurs. For large polarons with wave functions distributed over many lattice sites, Fröhlich et al. formulated a comprehensive quantum-mechanical description.<sup>93</sup> Feynman further built upon the work of Landau and Fröhlich with a variational approach to give an accurate coupling constant to quantify this interaction<sup>121</sup> as given by

$$\alpha_{\text{F}} = \frac{e^2}{\hbar} \left( \frac{1}{\epsilon_{\infty}} - \frac{1}{\epsilon_0} \right) \sqrt{\frac{m}{2\hbar\omega}} \quad (4)$$

where  $e$  is the electron's charge and  $\hbar$  is Planck's reduced constant;  $\epsilon_{\infty}$  and  $\epsilon_0$  are the high-frequency and static dielectric constants, respectively;  $m$  is the effective mass of the charge carrier; and  $\omega$  is the LO phonon frequency. Note that, typically in the weak coupling regime where  $\alpha_{\text{F}} \leq 2$ , large polaron formation occurs.<sup>122</sup>

Holstein, on the other hand, pioneered the investigation on the small polarons that appear because of the strong and short-range electron–phonon coupling.<sup>117</sup> The Holstein model has been successfully applied to a wide range of properties, from superconductivity to thermoelectric properties to carrier mobilities.<sup>123–127</sup> More recently, coupling between electrons and phonons as well as the polaronic charge transport through molecular crystals has also been investigated by this model.<sup>128,129</sup> Here in the Holstein Hamiltonian the electron–phonon interaction parameter explicitly couples electronic and phonon subsystems.<sup>117,130</sup> While an exact solution of this model is challenging, the perturbative approaches have been broadly used to describe both strong and weak electron–phonon coupling limits.<sup>129,131,132</sup>

In semiconductor devices, polarons may exist as defects.<sup>123,127</sup> Defects are ubiquitous in semiconductor engineering where it is well-known that electronic properties may be tuned by introducing intentional defects through doping. Polarons can appear because of doping or charge injection or be created through the separation of an exciton formed through electronic excitation. Once the polaron is formed, the dynamics of the lattice modulates its motion. Beyond scattering and electron–phonon coupling, polarons are distinguished in semiconductors by their size. Large polarons move coherently and slowly with a large effective mass through



scattering events that occur as nearby ions shift from their equilibrium because of the presence of the polaron.<sup>120</sup> Small polarons, conversely, move incoherently with a small effective mass through a hopping mechanism.<sup>123</sup> Though, as mentioned before, a polaron may begin large and through the loss of coherence become localized, and vice versa, a small polaron may become large if its mean-free-path becomes long. Theoretical and experimental studies extensively investigated polaronic effects in various devices. Polarons can, for instance, increase nonradiative recombination or create charge transport pathways across multiple unit cells (or grain boundaries), which enhance charge mobility, depending on the application.<sup>128,133–135</sup> Light-harvesting applications, e.g., photovoltaics, require the minimization of nonradiative recombination and impedance across the grain boundaries in the material to ensure maximum collection of photoexcited electrons. Light-emission applications, on the other hand, rely on the maximization of the radiative recombination of electrons and holes in the emissive layer aiming for maximum emission efficiency.

Polaron dynamics can be modeled from first principles aiming to guide experimentalists in the engineering of the most efficient devices for each application based on the expected polaronic behavior in the materials.<sup>136,137</sup> In realistic materials, depending on the bonding characteristics, either ionic or covalent bonding has been treated using nonperturbative DFT or density functional perturbation theory (DFPT), respectively, to model the mobility of a polaron.<sup>138</sup> Ionic materials tend to have large Fröhlich coupling constants, indicating incoherent, low mobility, small polaron transport, as the coupling constant is inversely proportional to the polaron mobility.<sup>93</sup> In covalent materials, the opposite is true. To model polaron mobility, the frequency-dependent and static dielectric constants, as well as the phonon frequency, must be determined using perturbation theory; the effective mass can be solved for nonperturbative approximation using parabolic band-fitting techniques. These calculated values are used to study both large and small polarons as the Boltzmann equation gives a limit for coherent transport, while the Fröhlich coupling constant provides a measure of electron–phonon coupling strength.<sup>139</sup>

**Polarons in MHPs.** In MHPs, polarons were studied using a combination of first-principles calculations and experimental spectroscopic methods.<sup>65–70,84,138,140–143</sup> The polaronic framework was drawn to explain a number of photophysical phenomena in devices like solar cells where superior performance surprised experimentalists, but also where degradation mechanisms and long-term stability continued to elude researchers.<sup>5</sup>

**Small Polarons in MHPs.** Small polaron formation has been hypothesized as a mechanism behind photodegradation and instability in MHP devices.<sup>35,66,69,145–153</sup> Light-activated metastable trap states with polaronic character have been identified as the origin of material degradation.<sup>35</sup> Localized charge states which strongly couple to local structural distortion result in macroscopic charge domains.<sup>35,65,148</sup> Formation of such domains further suppresses the efficient charge extraction from absorbing layers of the solar cell devices.<sup>149,150</sup> Small polarons are also understood as minority carriers that can cause shifted near-infrared absorption edge.<sup>35</sup> The formation of small polarons in MHPs has been studied both from first-principles modeling and spectroscopy-based experiments.<sup>143</sup> Beginning with the archetypal halide perov-

skite, MAPbI<sub>3</sub>, DFT simulations were performed to propose the small polaron formation due to the volumetric strain and reorientation of MA cations in this material.<sup>97</sup> Creation of small polarons involves the effect of cationic reorientation where MA molecules are rotated toward an electron residing on Pb atoms.<sup>151</sup> As shown in Figure 5, the spin densities of

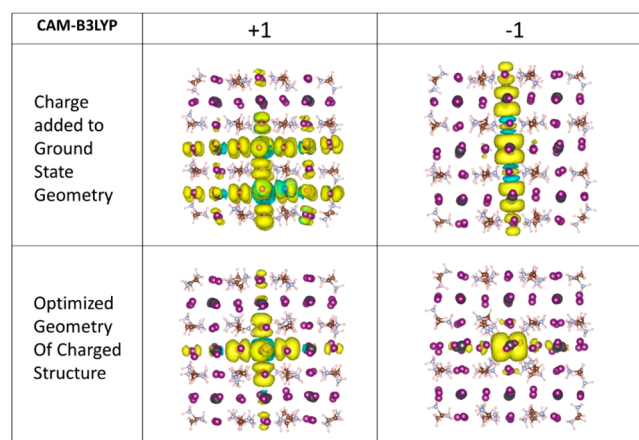


**Figure 5.** Small polaron modeling in MHPs. Spin density distribution for the hole (left) and electron (right) in optimized neutral (top panel) and optimized charged (bottom panel) structures of MAPbI<sub>3</sub> clusters. Here, the spin density signifies the distribution of extra electrons or holes in the lattice. Reproduced from ref 97. Copyright 2016 American Chemical Society.

positively charged (i.e., with an extra hole) optimized clusters exhibit an increase in the hole localization. Moreover, the negatively charged (i.e., with an extra electron) cluster demonstrates dramatic localization of electrons with geometry optimization. The polaron binding energies have been quantified as the energy difference between the charged system at the neutral geometry and the relaxed charge geometry. The calculation finds substantially high electron polaron binding energy (1.38 eV) compared to the hole (0.58 eV). To separate the contribution from MA cation orientation and volumetric strain to polaron binding, the study further investigates the binding energies in the CsPbI<sub>3</sub> cluster. Both the electron and hole binding energies appear to be substantially smaller for CsPbI<sub>3</sub>, 0.92 and 0.27 eV, respectively. Thus, cooperative interaction between volumetric strain and cationic orientations has been found to be the key ingredient for small polaron formation in hybrid halide perovskites.<sup>97</sup>

Experimentally, signatures of small polarons were detected with optical spectroscopy methods, and small polaron mitigation has, as was guided by computational efforts, been seen through cation, metal, and anion mixing.<sup>152</sup> Trapped states have been measured as a broad, low-energy peak in single-crystal MHP films using time-resolved and steady-state photoluminescence measurements, much like in polycrystalline surface states.<sup>153</sup> Capacitance–voltage measurements after light soaking at 1 Sun for 2 h show an increase in space charge density by an order of magnitude, suggesting the presence of trapped charges;<sup>35</sup> this is also evidenced using photocurrent transient measurements to show an increase of discharge time with constant illumination. Temperature-dependent optical density studies show that smaller halides have larger, temperature-independent exciton binding energies, whereas larger halides have smaller exciton binding energies which decrease with an increase in temperature.<sup>154</sup> Small

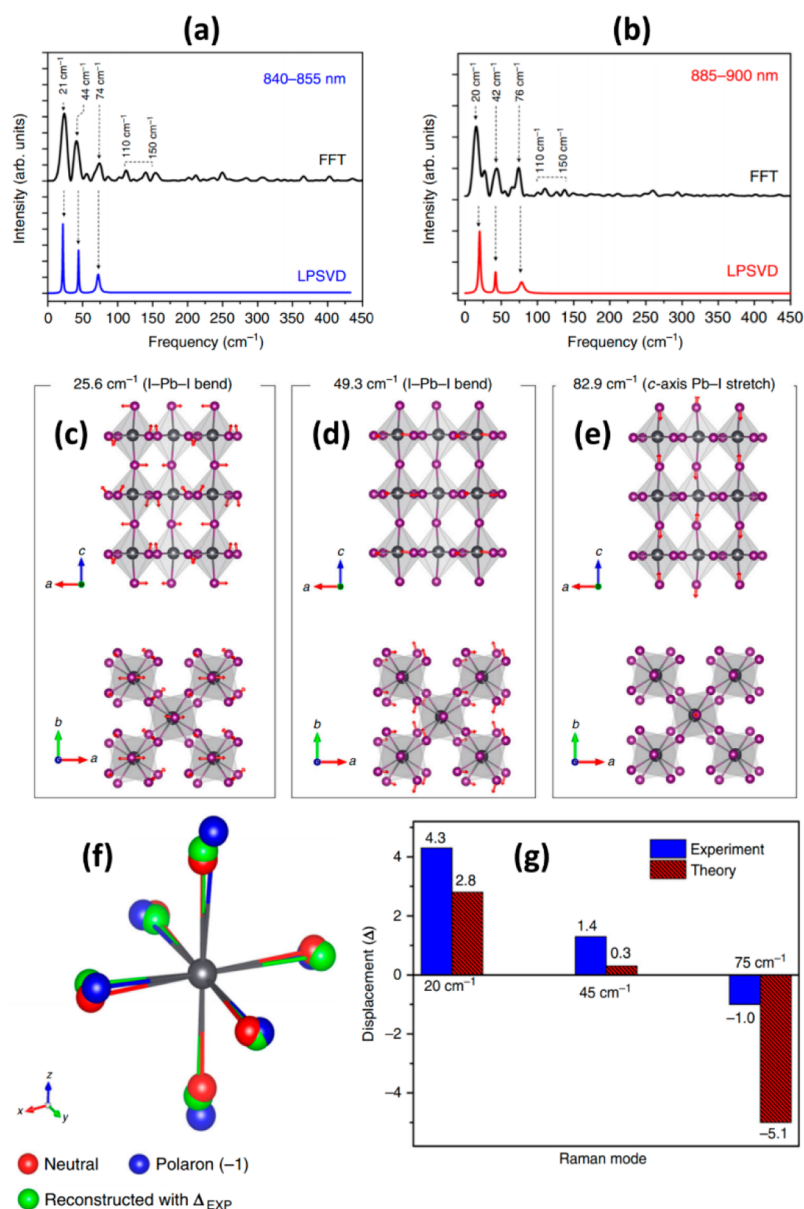


**Figure 6.** Time-resolved Raman spectroscopy analysis of near IR and IR region using Fourier and linear prediction methods to resolve vibrational modes in MAPI. Spectra from fast Fourier transform (FFT) (red line) and linear prediction with singular value decomposition (LPSVD) (blue line) analyses measured at (a) 840–855 nm and (b) 885–900 nm. (c–e) Computationally simulated vibrational modes of MAPI. (c) I–Pb–I bending mode of the  $\text{PbI}_6^{4-}$  octahedron at  $25.6 \text{ cm}^{-1}$ . (d) I–Pb–I bending on the  $ab$ -crystal plane at  $49.3 \text{ cm}^{-1}$ . (e) Pb–I stretching motion along the  $c$ -axis at  $82.0 \text{ cm}^{-1}$ . Red arrows placed on the atoms designate the direction and relative amplitude of displacements in a vibrational mode. (f and g) Geometric comparisons between experimental and computational results. (f)  $\text{PbI}_6^{4-}$  octahedral geometry from the experiment (green) and computationally calculated neutral (red) and polaron (blue) state structures. (g) Comparisons in displacement between the experiment and computation. Reproduced from ref 143. Copyright 2018 Nature Research.

polarens have also been probed in lower-dimensional MHPs using femtosecond transient absorption measurements which show kinetics indicative of small polaron formation.<sup>71</sup> As an example, recently, the experimental evidence for polaron formation in 3D  $\text{MAPbI}_3$  has been demonstrated by Park et al.<sup>143</sup> The femtosecond impulsive stimulated Raman spectroscopy has been applied to measure the low-frequency oscillation of coherent vibrational wave packets. By probing the oscillatory signals in the transient neutral excited-state absorption band near-infrared wavelength and further performing the detailed frequency analyses, low-frequency vibrational modes at  $\sim 20$ ,  $\sim 43$ , and  $\sim 75 \text{ cm}^{-1}$  have been identified (see Figure 6a,b). Concomitant DFT-based computational simulations find that

these vibrational normal modes mostly originate from I–Pb–I bond bending and stretching motions, whereas other higher-frequency Raman modes above  $\sim 100 \text{ cm}^{-1}$  involve MA cation dynamics (Figure 6c–e).<sup>143</sup> The neutral excited-state structure with electron polaron and associated atomic displacements in inorganic Pb/I cages have further been simulated by DFT-based computations (Figure 6f,g). The distorted geometry near polarons shows elongated  $\text{PbI}_6$  octahedra along the  $z$ -axis and bent Pb–I–Pb angles. Experimentally, the changes in neutral excited-state geometries have been quantified by exploring time-dependent Raman intensities. Good qualitative agreements between the experimental and computationally calculated displacements of these low-frequency models quantify



dynamical distortions of the Pb/I structure, indicating that the polaronic state coherently generates following electronic excitations in 3D MAPbI<sub>3</sub> (Figure 6g).<sup>143</sup>

In a subsequent elaborate study, the isolated clusters of (MA/FA/Cs)Pb(I/Br)<sub>3</sub> perovskites have been explored computationally to understand how polaron formation is affected by composition, lattice symmetry, electronic character, and electron–phonon interactions.<sup>141</sup> For all these materials, the electron polarons consistently exhibit stronger binding compared to hole polarons. Small electron polaron formation also results in Jahn–Teller-like distortions in the metal halide octahedra as found for MAPbI<sub>3</sub>.<sup>97</sup> On the other hand, the hole polarons contract the octahedra uniformly. Such distinct structural changes with electron and hole polaron formation can further be used to identify and manipulate the polaronic phenomena in hybrid perovskites. The study found that electron polaron binding weakens as A-cations change from MA to Cs to FA. As FA and Cs have much smaller or zero dipole moments compared to the larger one of MA, the cationic reorientational contributions to polaron stabilization are far less for FA- and Cs-based perovskites.<sup>141</sup> The Br-based perovskites further demonstrate higher electron and smaller hole polaron binding energies compared to iodine-based materials. Interestingly, it has also been found that upon replacing Pb with Sn in MABl<sub>3</sub> (B = Sn or Pb) the electron and hole polaron become weakly bound. This invaluable information provides the relation between chemical components and polaron binding in halide perovskites, allowing one to design materials with controlled polaronic features.<sup>141</sup>

The strong dependence of polaron binding energies on the composition of halide perovskites further motivates computational study to explore the effect of cation alloying on this subject.<sup>155</sup> Precise A-cation alloying has been demonstrated to enhance the stability of halide perovskites against phase transition as well as improves their photovoltaic performances compared to monocationic counterparts.<sup>37,75,76,156–160</sup> Alloying Cs and MA with FA cations in FA<sub>0.69</sub>MA<sub>0.25</sub>Cs<sub>0.06</sub>PbI<sub>3</sub> demonstrate a reduction in both hole and electron polaron binding energies.<sup>65</sup> The spatial delocalization of extra charges is found to be more delocalized in this lattice compared to monocationic perovskites. The cation mixing breaks down the local symmetry preventing the cooperative cation reorientation, which has been identified as one of the major contributors to the polaron binding in MAPbI<sub>3</sub>. Additionally, the contracted low-symmetry lattice of the mixed cation perovskites exhibits more structural rigidity, demonstrating resistance toward structural distortions particularly to Pb–I bond elongations, which are prerequisite to the formation of electron polaronic states in halide perovskites.<sup>76</sup> Smaller geometric change in mixed A-cation halide perovskites also indicates that experimental identification of polaron formation in these lattices will be difficult. Thus, cation alloying has been argued to be an efficient approach to partially mitigate small polaron formation in halide perovskites and consequently improve their charge separation, transport, and carrier collection in optoelectronic device architectures.<sup>65</sup>

**Large Polarons in MHPs.** As a mobile charge carrier moves through an MHP, competing dynamics occur between the rotation of the organic cation sublattice and the phonon modes of the metal-halide sublattice. As we discussed, the rotation of the organic cations tends to stabilize and localize a charge while the phonons of the inorganic cage tend to further localize but also transport the carrier. With binding energy below  $k_B T$

and a subpicosecond formation time, the carrier forms a large polaron. With a long coherence length, the stabilized large polaron effectively screens other mobile charges from scattering in an MHP.

By solving eq 4 using, for instance, a tight-binding model,<sup>142</sup> one sees that MHPs have a Fröhlich coupling constant similar to other ionic halide salts, indicating the existence of moderate to strong electron–phonon coupling. Despite measurements of modest carrier mobility at high temperature,<sup>161</sup> large carrier diffusion lengths and lifetimes, low recombination rates, and low hot carrier scattering rates have been measured in MHPs; large polaron formation has also been used to explain these anomalies.<sup>43,48,52,66,85,142,162–165</sup> Figure 7 shows temperature-

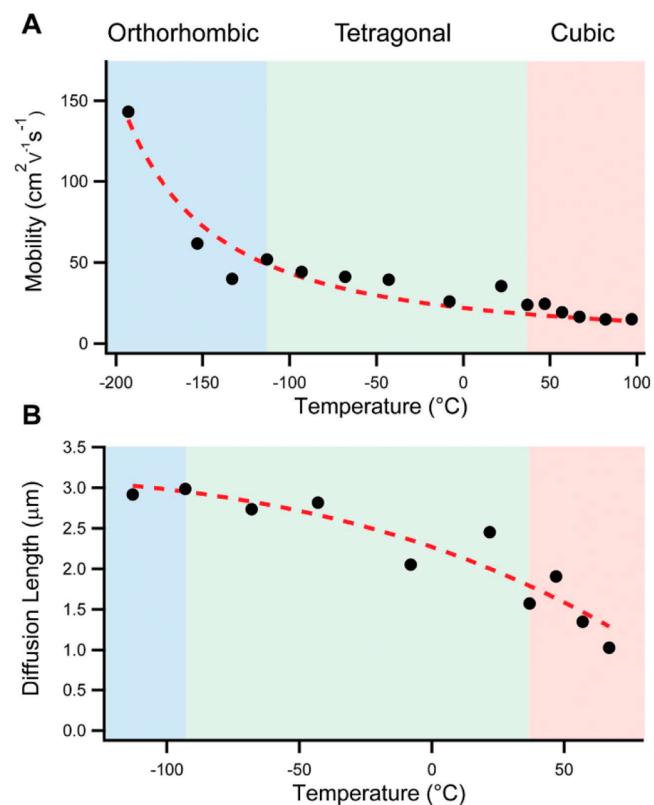


**Figure 7.** Temperature-dependent (a) mobility and (b) diffusion length for MAPbI<sub>3</sub> using optical-pump THz spectroscopy. The dashed line is the theoretical fit of a  $T^{-3/2}$  dependence. Reproduced from ref 86. Copyright 2015 Wiley.

dependent mobility and diffusion length measurements that indicate while the mobility decreases at higher temperature, the diffusion length of carriers is still well above the optical absorption depth ( $L_D \approx 1 \mu\text{m}$ ).<sup>86</sup>

Ultrafast THz spectroscopy has been used to measure large polarons in CsPbBr<sub>3</sub> to study the material's dielectric response, verifying electron–phonon assisted charge transport;<sup>68</sup> this type of spectroscopy also verified the signatures of Rashba splitting in MHPs from measurements of the circular photogalvanic effect.<sup>144</sup> The femtosecond optical Kerr effect spectroscopy was used for single-crystal MHPs to show large polaron formation after carrier injection due to optical excitation with formation constants ranging from 0.6 to 0.26 ps (Figure 8).<sup>140</sup>

The large polaron effective mass has been calculated in MHPs using momentum relaxation time or mean-free path

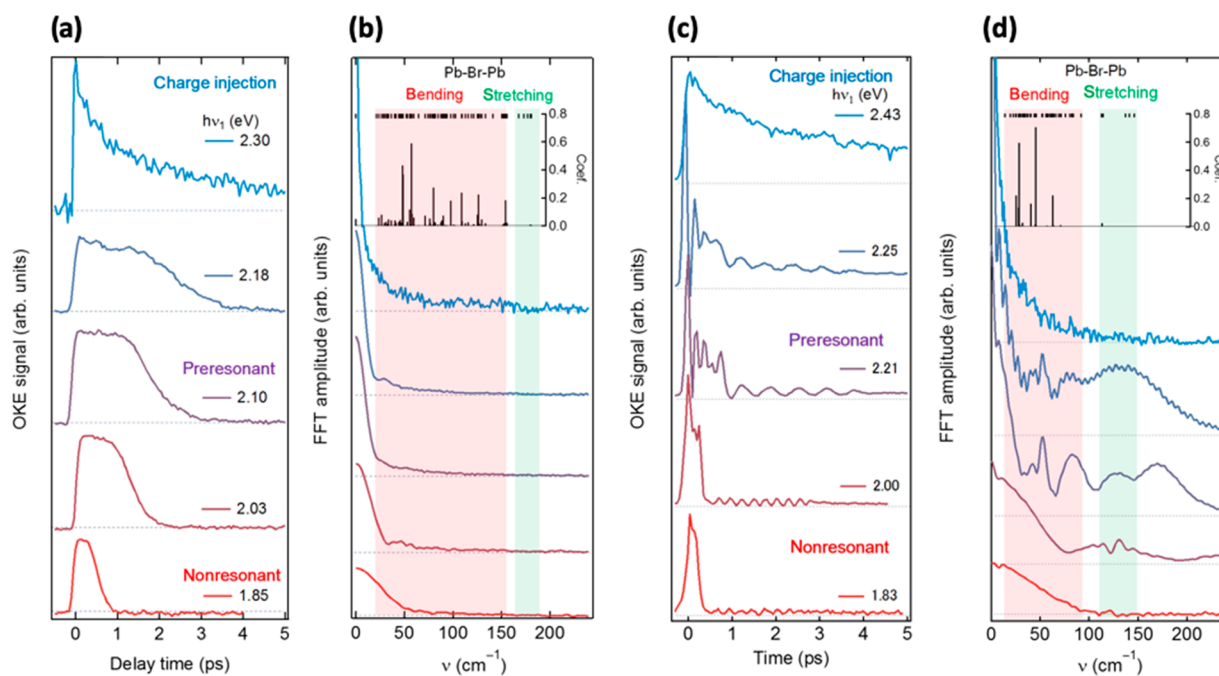


**Figure 8.** Time-resolved optical Kerr effect (a and c) spectroscopy signal and (b and d) fast Fourier transform of the spectra for (a and b) MAPbBr<sub>3</sub> and (c and d) CsPbBr<sub>3</sub>. Black bars in panel b represent the extracted Fourier coefficients. Reproduced from ref 140. Copyright 2017 AAAS.

methods to calculate the mobility and thus the effective mass by<sup>166</sup>

$$m^* = \frac{(e\lambda)^2}{2k_B T \mu^2} \quad (5)$$

where  $e$  is the electron charge,  $m^*$  the effective mass,  $\lambda$  the mean-free path,  $\mu$  the mobility, and  $k_B T$  the thermal energy. Using a value of 10 lattice constants for the mean free path along with a range of mobility from 10 to 60 cm<sup>2</sup> V<sup>-1</sup> s<sup>-1</sup> results in a range of room-temperature effective masses of 10–300 $m_e$ , where  $m_e$  is the mass of a free electron. This large effective mass, especially compared to the single-particle band effective mass ( $\sim 0.1m_e$ ) indicates that large polarons in MHPs form and effectively screen other mobile charges from scattering with LO phonons. Recent DFT calculations<sup>70</sup> reported the distribution of a large polaron across multiple lattice constants, indicating screened pathways for mobile charge carriers shown in Figure 9. Here the largest displacements of the metal-halide framework occur near the center of the large polaron where phonon-modes assist the motion of screened mobile charge carriers.

The large effective mass can also explain the slow cooling of hot electrons due to similar screening processes<sup>138,159,169–171</sup>, something that was seen in transient absorption spectroscopy measurements.<sup>88</sup> These hot carrier dynamics were also studied from first-principles calculations where a phonon bottleneck due to the overlap of large polaron wave functions slows the thermalization of above-bandgap photoelectrons.<sup>167</sup> These results imply that hot carrier extraction may be possible in MHP photovoltaics.

Exceptional power conversion efficiency and a low recombination rate in MHPs have also been attributed to large polaron formation where the large static dielectric response causes repulsion to occur between oppositely charged large polarons (electrons and holes).<sup>168</sup> Calculations of the

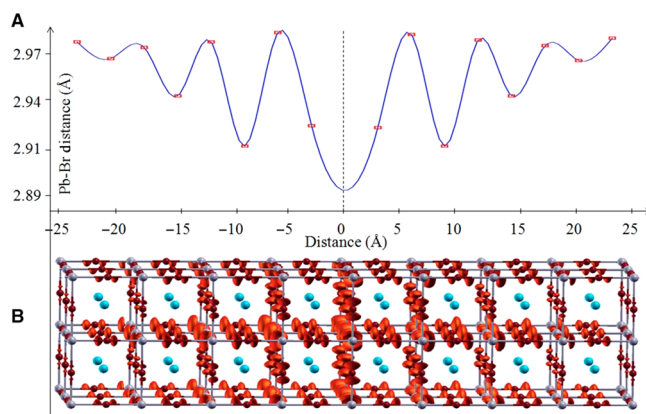


**Figure 9.** (a) Change in metal-halide bond length and (b) charge density distribution due to large polaron formation in CsPbBr<sub>3</sub>. Reproduced from ref 70. Copyright 2017 AAAS.

Detailed studies suggest that compositional engineering, particularly controlled mixing of differently sized A-cations, can partially mitigate the small polaron formation and enhance the stability of halide perovskites against degradation.

Fröhlich electron–phonon coupling model revealed that MHPs' large static dielectric constant causes long-range interactions between electronic charge carriers and the displacement of ions from their equilibrium positions. As these large polarons form, they disperse through the lattice, and the distortion created by different carriers interferes.

Figure 10 shows that at small separations between oppositely charged large polarons when their interference overlaps, a

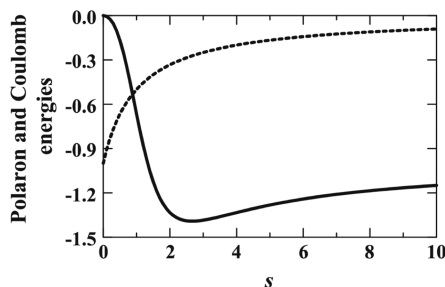


**Figure 10.** Total polaron (solid line) and Coulomb attraction (dotted line) energy for two oppositely charged large polarons as a function of their separation  $s$ . Reproduced from ref 168. Copyright 2018 AIP Publishing.

repulsion force occurs that is stronger than the attractive Coulomb force. This repulsion can then slow recombination between these self-trapped states where an energy barrier exists at small distances dependent upon the motion of the surrounding ions.<sup>168</sup>

As with small polarons, mixing the cation and halide atoms in MHPs was proposed as a mechanism to enhance the stability of large polaron formation.<sup>70</sup> This implies that charge screening due to the large polaron formation is another tunable parameter in MHPs. Moreover, as is seen in many semiconducting materials, a small polaron may be delocalized and become a large polaron in MHPs. This ability to tune the size of polarons, an important task in developing stable devices, was shown by Zhou et al.<sup>65</sup> through cation mixing in MHPs. A recent study<sup>142</sup> further suggested that in the benchmark MAPI perovskite, large polaron formation can occur when both dynamic disorders from the MA dipole and lattice reorientation of the  $\text{PbI}_3$  sublattice work to enhance the electron mobility. This indicates that both steric and temperature-based effects may be used to engineer devices that enhance carrier mobility in MHPs.

In conclusion, this Perspective summarizes different proposed charge-transport mechanisms for halide perovskites with a focus on the polaronic character of carriers. Exploring both small and large polarons in MHPs, we discuss their formation and effect on structural and carrier dynamics in these photoactive materials. Lattice distortion due to small polaron formation has been identified by recent Raman-spectroscopy-based experimental work and is predicted to be a probable reason for reversible photodegradation in these halide perovskites because of the formation of static charge pools. Strong coupling between soft structure and excess charges results in Jahn–Teller distortion in the octahedral framework of lead halides. Detailed studies further suggest that compositional engineering, particularly controlled mixing of differently sized A-cations, can partially mitigate the small polaron formation and enhance the stability of halide perovskites against degradation. Furthermore, electron–phonon coupling in the ionic lattices of MHPs and the dominant presence of long-range Coulomb potentials indicate the large polarons in these materials are a dominant charge carrier. Such polaron formations can protect the photogenerated electrons and holes from recombination and defect-scattering, eventually providing long carrier lifetime and large diffusion length, as found in MHPs. The higher effective mass of large polarons further

reduces the electron–LO phonon scattering, and that can result in slow cooling of hot carriers in these perovskites. The heavy, large polarons in MHPs also explain the modest mobility of these materials despite having very small single-particle band-edge effective masses for carriers. Regardless of recent advancements in the fundamental understanding of polaron-dominated charge dynamics, the influences of structural irregularities such as grain boundaries and interfaces, light-illumination in the polaronic transport is yet to be explored. More advanced spectroscopic and optical experiments along with cutting-edge *ab initio* computational simulations in large computational cells are necessary to investigate these complex interactions at the atomistic level.

## AUTHOR INFORMATION

### Corresponding Author

**Sergei Tretiak** – Theoretical Division, Center for Nonlinear Studies, and Center for Integrated Nanotechnologies, Los Alamos National Laboratory, Los Alamos, New Mexico 87545, United States; [orcid.org/0000-0001-5547-3647](https://orcid.org/0000-0001-5547-3647); Email: [serg@lanl.gov](mailto:serg@lanl.gov)

### Authors

**Dibyajyoti Ghosh** – Theoretical Division and Center for Nonlinear Studies, Los Alamos National Laboratory, Los Alamos, New Mexico 87545, United States; [orcid.org/0000-0002-3640-7537](https://orcid.org/0000-0002-3640-7537)

**Eric Welch** – Material Science, Engineering and Commercialization Department and Department of Physics, Texas State University, Texas 78666, United States; [orcid.org/0000-0002-8066-8005](https://orcid.org/0000-0002-8066-8005)

**Amanda J. Neukirch** – Theoretical Division, Los Alamos National Laboratory, Los Alamos, New Mexico 87545, United States; [orcid.org/0000-0002-6583-0086](https://orcid.org/0000-0002-6583-0086)

**Alex Zakhidov** – Material Science, Engineering and Commercialization Department and Department of Physics, Texas State University, Texas 78666, United States; [orcid.org/0000-0001-6980-2659](https://orcid.org/0000-0001-6980-2659)

Complete contact information is available at: <https://pubs.acs.org/10.1021/acs.jpcllett.0c00018>

### Author Contributions

<sup>#</sup>D.G. and E.W. contributed equally.

### Notes

The authors declare no competing financial interest.

### Biographies

**Dibyajyoti Ghosh** finished his Ph.D. at JNCASR, Bangalore in 2016. For his Ph.D., he worked on electron, spin, and heat transport through molecular nanojunctions and low-dimensional layered materials. After his Ph.D., he moved to the University of Bath, U.K. as a Post-Doctoral Research Associate for 2 years to work on photovoltaic properties and ion dynamics in new-generation optoelectronic materials. At present, he is a Research Associate at Los Alamos National Laboratory, United States. His current research interests include investigating charge carrier dynamics, defect properties, and accelerated materials design and discovery for solar cells, LEDs, and high-energy radiation detectors.

**Eric Welch** received his Ph.D. from Texas State University in San Marcos, TX in 2019. He studied the optoelectronic properties of halide perovskites using first principles, density functional theory methods. He currently works as a postdoctoral researcher in the group of Dr. Shane Yost in the Chemistry and Biochemistry department at



Texas State University studying charge transfer and electronic coupling while developing the QChem code. His current research interests are ALMO-NOCI-MP2 calculations of electronic coupling parameters in DNA base pairs.

**Dr. Amanda Neukirch** received her Physics Ph.D. in 2014 from the University of Rochester (United States). She was then a Director-funded postdoctoral fellow at LANL (2014–2017) before becoming a LANL staff scientist in 2017. Her research is focused on modeling the electronic and optical properties of organic molecules, semiconductor nanoparticles, and mixed halide perovskites for applications in optoelectronic devices such as solar cells, LEDs, detectors, and various chemical and biosensors.

**Dr. Alex Zakhidov** received his Physics doctorate in 2006 from the Moscow State University, Russia. He then was a postdoctoral research at Cornell University (2006–2009); Humboldt postdoc fellow in Dresden, Germany (2010); and a group leader at Fraunhofer COMEDD, Dresden Germany (2010–2013). In 2014 Dr. Zakhidov joined Texas State University as an assistant professor of Physics. His research is focused on organic and hybrid disordered systems, including fundamentals, processing, mechanisms, and applications in optoelectronic devices such as solar cells, LEDs, transistors, lasers, nonvolatile memory, and various chemical and biosensors.

**Sergei Tretiak** received his Chemistry doctorate in 1998 from the University of Rochester (United States). He was then a Director-funded postdoctoral fellow (1999–2001) and subsequently became a staff scientist at LANL and a member of the DOE-funded Center for Integrated Nanotechnologies (CINT). Tretiak also serves as Adjunct Professor at the University of California, Santa Barbara (UCSB) (2015 to present) and at Skolkovo Institute of Science and Technology, Skoltech, Russia (2013 to present). His research interests include development of electronic structure methods for molecular optical properties, nonlinear optical response of organic chromophores, nonadiabatic dynamics of electronically excited states, optical response of confined excitons in conjugated polymers, carbon nanotubes, semiconductor nanoparticles, mixed halide perovskites and molecular aggregates, and the use of machine learning and data science toward modeling electronic and chemical properties.

## ACKNOWLEDGMENTS

The work at Los Alamos National Laboratory (LANL) was supported by the LANL LDRD program. This work was done in part at the Center for Nonlinear Studies (CNLS) and the Center for Integrated Nanotechnologies (CINT), a U.S. Department of Energy and Office of Basic Energy Sciences user facility, at LANL. This research used resources provided by the LANL Institutional Computing Program. Los Alamos National Laboratory is operated by Triad National Security, LLC, for the National Nuclear Security Administration of the U.S. Department of Energy (Contract No. 89233218NCA000001). E.W. and A.Z. acknowledge LANL CINT for the access to the HPC cluster. This work was in part funded by Department of Navy's (DoN) HBCU/MI Program, ONR Grant Number N00014-19-S-F004.

## REFERENCES

(1) Kojima, A.; Teshima, K.; Shirai, Y.; Miyasaka, T. Organometal Halide Perovskites as Visible-Light Sensitizers for Photovoltaic Cells. *J. Am. Chem. Soc.* **2009**, *131* (17), 6050–6051.

(2) Lee, M. M.; Teuscher, J.; Miyasaka, T.; Murakami, T. N.; Snaith, H. J. Efficient Hybrid Solar Cells Based on Meso-Superstructured Organometal Halide Perovskites. *Science (Washington, DC, U. S.)* **2012**, *338* (6107), 643–647.

(3) Green, M. A.; Ho-Baillie, A.; Snaith, H. J. The Emergence of Perovskite Solar Cells. *Nat. Photonics* **2014**, *8* (7), 506–514.

(4) Grätzel, M. The Rise of Highly Efficient and Stable Perovskite Solar Cells. *Acc. Chem. Res.* **2017**, *50* (3), 487–491.

(5) Dou, L.; Yang, Y. M.; You, J.; Hong, Z.; Chang, W.-H.; Li, G.; Yang, Y. Solution-Processed Hybrid Perovskite Photodetectors with High Detectivity. *Nat. Commun.* **2014**, *5*, 5404.

(6) Snaith, H. J. Present Status and Future Prospects of Perovskite Photovoltaics. *Nat. Mater.* **2018**, *17* (5), 372.

(7) Eperon, G. E.; Leijtens, T.; Bush, K. A.; Prasanna, R.; Green, T.; Wang, J. T.-W.; McMeekin, D. P.; Volonakis, G.; Milot, R. L.; May, R.; et al. Perovskite-Perovskite Tandem Photovoltaics with Optimized Band Gaps. *Science (Washington, DC, U. S.)* **2016**, *354* (6314), 861–865.

(8) Jena, A. K.; Kulkarni, A.; Miyasaka, T. Halide Perovskite Photovoltaics: Background, Status, and Future Prospects. *Chem. Rev.* **2019**, *119* (5), 3036–3103.

(9) Brenner, T. M.; Egger, D. A.; Kronik, L.; Hodes, G.; Cahen, D. Hybrid Organic - Inorganic Perovskites: Low-Cost Semiconductors with Intriguing Charge-Transport Properties. *Nat. Rev. Mater.* **2016**, *1* (1), 15007.

(10) Buizza, L. R. V.; Crothers, T. W.; Wang, Z.; Patel, J. B.; Milot, R. L.; Snaith, H. J.; Johnston, M. B.; Herz, L. M. Charge-Carrier Dynamics, Mobilities, and Diffusion Lengths of 2D–3D Hybrid Butylammonium–Cesium–Formamidinium Lead Halide Perovskites. *Adv. Funct. Mater.* **2019**, *29*, 1902656.

(11) Biewald, A.; Giesbrecht, N.; Bein, T.; Docampo, P.; Hartschuh, A.; Ciesielski, R. Temperature-Dependent Ambipolar Charge Carrier Mobility in Large-Crystal Hybrid Halide Perovskite Thin Films. *ACS Appl. Mater. Interfaces* **2019**, *11* (23), 20838–20844.

(12) Castelli, I. E.; García-Lastra, J. M.; Thygesen, K. S.; Jacobsen, K. W. Bandgap Calculations and Trends of Organometal Halide Perovskites. *APL Mater.* **2014**, *2* (8), 081514.

(13) Ruf, F.; Aygüler, M. F.; Giesbrecht, N.; Rendenbach, B.; Magin, A.; Docampo, P.; Kalt, H.; Hetterich, M. Temperature-Dependent Studies of Exciton Binding Energy and Phase-Transition Suppression in (Cs, FA, MA)Pb(I, Br)<sub>3</sub> Perovskites. *APL Mater.* **2019**, *7* (3), 031113.

(14) Galkowski, K.; Mitioglu, A.; Miyata, A.; Plochocka, P.; Portugall, O.; Eperon, G. E.; Wang, J. T. W.; Stergiopoulos, T.; Stranks, S. D.; Snaith, H. J.; et al. Determination of the Exciton Binding Energy and Effective Masses for Methylammonium and Formamidinium Lead Tri-Halide Perovskite Semiconductors. *Energy Environ. Sci.* **2016**, *9* (3), 962–970.

(15) Yu, W.; Jiang, Y.; Zhu, X.; Luo, C.; Jiang, K.; Chen, L.; Zhang, J. Diversity of Band Gap and Photoluminescence Properties of Lead Halide Perovskite: A Halogen-Dependent Spectroscopic Study. *Chem. Phys. Lett.* **2018**, *699*, 93–98.

(16) Sherkar, T. S.; Momblona, C.; Gil-Escrig, L.; Ávila, J.; Sessolo, M.; Bolink, H. J.; Koster, L. J. A. Recombination in Perovskite Solar Cells: Significance of Grain Boundaries, Interface Traps, and Defect Ions. *ACS Energy Lett.* **2017**, *2* (4), 1214.

(17) Ball, J. M.; Petrozza, A. Defects in Perovskite-Halides and Their Effects in Solar Cells. *Nat. Energy* **2016**, *1* (11), 16149.

(18) NREL. Best Research-Cell Efficiency Chart. Photovoltaic Research. <https://www.nrel.gov/pv/cell-efficiency.html> (accessed 19-09-2019).

(19) Zhang, X.; Liu, H.; Wang, W.; Zhang, J.; Xu, B.; Karen, K. L.; Zheng, Y.; Liu, S.; Chen, S.; Wang, K.; et al. Hybrid Perovskite Light-Emitting Diodes Based on Perovskite Nanocrystals with Organic-Inorganic Mixed Cations. *Adv. Mater.* **2017**, *29* (18), 1606405.

(20) Tan, Z.-K.; Moghaddam, R. S.; Lai, M. L.; Docampo, P.; Higler, R.; Deschler, F.; Price, M.; Sadhanala, A.; Pazos, L. M.; Credgington, D.; et al. Bright Light-Emitting Diodes Based on Organometal Halide Perovskite. *Nat. Nanotechnol.* **2014**, *9* (9), 687.

(21) Yuan, M.; Quan, L. N.; Comin, R.; Walters, G.; Sabatini, R.; Voznyy, O.; Hoogland, S.; Zhao, Y.; Beauregard, E. M.; Kanjanaboos, P.; et al. Perovskite Energy Funnel for Efficient Light-Emitting Diodes. *Nat. Nanotechnol.* **2016**, *11* (10), 872.

- (22) Kim, Y.-H.; Cho, H.; Heo, J. H.; Kim, T.-S.; Myoung, N.; Lee, C.-L.; Im, S. H.; Lee, T.-W. Multicolored Organic/Inorganic Hybrid Perovskite Light-Emitting Diodes. *Adv. Mater.* **2015**, *27* (7), 1248–1254.
- (23) Smith, M. D.; Connor, B. A.; Karunadasa, H. I. Tuning the Luminescence of Layered Halide Perovskites. *Chem. Rev.* **2019**, *119* (5), 3104–3139.
- (24) Jaffe, A.; Lin, Y.; Beavers, C. M.; Voss, J.; Mao, W. L.; Karunadasa, H. I. High-Pressure Single-Crystal Structures of 3D Lead-Halide Hybrid Perovskites and Pressure Effects on Their Electronic and Optical Properties. *ACS Cent. Sci.* **2016**, *2* (4), 201–209.
- (25) Fang, Y.; Dong, Q.; Shao, Y.; Yuan, Y.; Huang, J. Highly Narrowband Perovskite Single-Crystal Photodetectors Enabled by Surface-Charge Recombination. *Nat. Photonics* **2015**, *9* (10), 679.
- (26) Ramasamy, P.; Lim, D. H.; Kim, B.; Lee, S. H.; Lee, M. S.; Lee, J. S. All-Inorganic Cesium Lead Halide Perovskite Nanocrystals for Photodetector Applications. *Chem. Commun.* **2016**, *52* (10), 2067–2070.
- (27) Hu, X.; Zhang, X.; Liang, L.; Bao, J.; Li, S.; Yang, W.; Xie, Y. High-Performance Flexible Broadband Photodetector Based on Organolead Halide Perovskite. *Adv. Funct. Mater.* **2014**, *24* (46), 7373–7380.
- (28) He, Y.; Matei, L.; Jung, H. J.; McCall, K. M.; Chen, M.; Stoumpos, C. C.; Liu, Z.; Peters, J. A.; Chung, D. Y.; Wessels, B. W.; et al. High Spectral Resolution of Gamma-Rays at Room Temperature by Perovskite CsPbBr<sub>3</sub> Single Crystals. *Nat. Commun.* **2018**, *9* (1), 1609.
- (29) Wei, H.; DeSantis, D.; Wei, W.; Deng, Y.; Guo, D.; Savenije, T. J.; Cao, L.; Huang, J. Dopant Compensation in Alloyed CH<sub>3</sub>NH<sub>3</sub>PbBr<sub>3-x</sub>Cl<sub>x</sub> Perovskite Single Crystals for Gamma-Ray Spectroscopy. *Nat. Mater.* **2017**, *16* (8), 826.
- (30) Yakunin, S.; Dirin, D. N.; Shynkarenko, Y.; Morad, V.; Cherniukh, I.; Nazarenko, O.; Kreil, D.; Nauser, T.; Kovalenko, M. V. Detection of Gamma Photons Using Solution-Grown Single Crystals of Hybrid Lead Halide Perovskites. *Nat. Photonics* **2016**, *10* (9), 585.
- (31) Berhe, T. A.; Su, W.-N.; Chen, C.-H.; Pan, C.-J.; Cheng, J.-H.; Chen, H.-M.; Tsai, M.-C.; Chen, L.-Y.; Dubale, A. A.; Hwang, B.-J. Organometal Halide Perovskite Solar Cells: Degradation and Stability. *Energy Environ. Sci.* **2016**, *9* (2), 323–356.
- (32) Boyd, C. C.; Cheacharoen, R.; Leijtens, T.; McGehee, M. D. Understanding Degradation Mechanisms and Improving Stability of Perovskite Photovoltaics. *Chem. Rev.* **2019**, *119* (5), 3418–3451.
- (33) Yang, J.; Siempelkamp, B. D.; Liu, D.; Kelly, T. L. Investigation of CH<sub>3</sub>NH<sub>3</sub>PbI<sub>3</sub> Degradation Rates and Mechanisms in Controlled Humidity Environments Using in Situ Techniques. *ACS Nano* **2015**, *9* (2), 1955–1963.
- (34) Misra, R. K.; Aharon, S.; Li, B.; Mogilyansky, D.; Visoly-Fisher, I.; Etagar, L.; Katz, E. A. Temperature- and Component-Dependent Degradation of Perovskite Photovoltaic Materials under Concentrated Sunlight. *J. Phys. Chem. Lett.* **2015**, *6* (3), 326–330.
- (35) Nie, W.; Blancon, J. C.; Neukirch, A. J.; Appavoo, K.; Tsai, H.; Chhowalla, M.; Alam, M. A.; Sfeir, M. Y.; Katan, C.; Even, J.; et al. Light-Activated Photocurrent Degradation and Self-Healing in Perovskite Solar Cells. *Nat. Commun.* **2016**, *7* (May), 1–9.
- (36) Bryant, D.; Aristidou, N.; Pont, S.; Sanchez-Molina, I.; Chotchanangatchaval, T.; Wheeler, S.; Durrant, J. R.; Haque, S. A. Light and Oxygen Induced Degradation Limits the Operational Stability of Methylammonium Lead Triiodide Perovskite Solar Cells. *Energy Environ. Sci.* **2016**, *9* (5), 1655–1660.
- (37) Ono, L. K.; Juarez-Perez, E. J.; Qi, Y. Progress on Perovskite Materials and Solar Cells with Mixed Cations and Halide Anions. *ACS Appl. Mater. Interfaces* **2017**, *9* (36), 30197–30246.
- (38) Jodlowski, A. D.; Roldán-Carmona, C.; Grancini, G.; Salado, M.; Ralaiarisoa, M.; Ahmad, S.; Koch, N.; Camacho, L.; De Miguel, G.; Nazeeruddin, M. K.; et al. Large Guanidinium Cation Mixed with Methylammonium in Lead Iodide Perovskites for 19% Efficient Solar Cells. *Nat. Energy* **2017**, *2* (12), 972.
- (39) Ghosh, D.; Walsh Atkins, P.; Islam, M. S.; Walker, A. B.; Eames, C. Good Vibrations: Locking of Octahedral Tilting in Mixed-Cation Iodide Perovskites for Solar Cells. *ACS Energy Lett.* **2017**, *2* (10), 2424.
- (40) Ghosh, D.; Aziz, A.; Dawson, J. A.; Walker, A. B.; Islam, M. S. Putting the Squeeze on Lead Iodide Perovskites: Pressure-Induced Effects To Tune Their Structural and Optoelectronic Behavior. *Chem. Mater.* **2019**, *31*, 4063.
- (41) Katan, C.; Mercier, N.; Even, J. Quantum and Dielectric Confinement Effects in Lower-Dimensional Hybrid Perovskite Semiconductors. *Chem. Rev.* **2019**, *119* (5), 3140–3192.
- (42) Manser, J. S.; Christians, J. A.; Kamat, P. V. Intriguing Optoelectronic Properties of Metal Halide Perovskites. *Chem. Rev.* **2016**, *116* (21), 12956–13008.
- (43) Egger, D. A.; Bera, A.; Cahen, D.; Hodes, G.; Kirchartz, T.; Kronik, L.; Lovrincic, R.; Rappe, A. M.; Reichman, D. R.; Yaffe, O. What Remains Unexplained about the Properties of Halide Perovskites? *Adv. Mater.* **2018**, *30*, 1800691.
- (44) Yu, Z.-G. Rashba Effect and Carrier Mobility in Hybrid Organic-Inorganic Perovskites. *J. Phys. Chem. Lett.* **2016**, *7*, 3078.
- (45) de Quillettes, D. W.; Frohna, K.; Emin, D.; Kirchartz, T.; Bulovic, V.; Ginger, D. S.; Stranks, S. D. Charge-Carrier Recombination in Halide Perovskites. *Chem. Rev.* **2019**, *119* (20), 11007–11019.
- (46) Shi, J.; Li, Y.; Li, Y.; Li, D.; Luo, Y.; Wu, H.; Meng, Q. From Ultrafast to Ultraslow: Charge-Carrier Dynamics of Perovskite Solar Cells. *Joule* **2018**, *2*, 879–901.
- (47) Herz, L. M. Charge-Carrier Mobilities in Metal Halide Perovskites: Fundamental Mechanisms and Limits. *ACS Energy Lett.* **2017**, *2* (7), 1539–1548.
- (48) Wright, A. D.; Verdi, C.; Milot, R. L.; Eperon, G. E.; Pérez-Osorio, M. A.; Snaith, H. J.; Giustino, F.; Johnston, M. B.; Herz, L. M. Electron-Phonon Coupling in Hybrid Lead Halide Perovskites. *Nat. Commun.* **2016**, *7*, 11755.
- (49) Davies, C. L.; Filip, M. R.; Patel, J. B.; Crothers, T. W.; Verdi, C.; Wright, A. D.; Milot, R. L.; Giustino, F.; Johnston, M. B.; Herz, L. M. Bimolecular Recombination in Methylammonium Lead Triiodide Perovskite Is an Inverse Absorption Process. *Nat. Commun.* **2018**, *9* (1), 293.
- (50) Wehrenfennig, C.; Eperon, G. E.; Johnston, M. B.; Snaith, H. J.; Herz, L. M. High Charge Carrier Mobilities and Lifetimes in Organolead Trihalide Perovskites. *Adv. Mater.* **2014**, *26* (10), 1584–1589.
- (51) Kim, H.-S.; Kim, S. K.; Kim, B. J.; Shin, K.-S.; Gupta, M. K.; Jung, H. S.; Kim, S.-W.; Park, N.-G. Ferroelectric Polarization in CH<sub>3</sub>NH<sub>3</sub>PbI<sub>3</sub> Perovskite. *J. Phys. Chem. Lett.* **2015**, *6* (9), 1729–1735.
- (52) Miyata, K.; Zhu, X. Y. Ferroelectric Large Polarons. *Nat. Mater.* **2018**, *17* (5), 379–381.
- (53) Liao, W. Q.; Zhang, Y.; Hu, C. L.; Mao, J. G.; Ye, H. Y.; Li, P. F.; Huang, S. D.; Xiong, R. G. A Lead-Halide Perovskite Molecular Ferroelectric Semiconductor. *Nat. Commun.* **2015**, *6*, 1–7.
- (54) Stroppa, A.; Di Sante, D.; Barone, P.; Bokdam, M.; Kresse, G.; Franchini, C.; Whangbo, M.-H.; Picozzi, S. Tunable Ferroelectric Polarization and Its Interplay with Spin-Orbit Coupling in Tin Iodide Perovskites. *Nat. Commun.* **2014**, *5*, 5900.
- (55) Frost, J. M.; Butler, K. T.; Walsh, A. Molecular Ferroelectric Contributions to Anomalous Hysteresis in Hybrid Perovskite Solar Cells. *APL Mater.* **2014**, *2* (8), 081506.
- (56) Zhao, T.; Shi, W.; Xi, J.; Wang, D.; Shuai, Z. Intrinsic and Extrinsic Charge Transport in CH<sub>3</sub>NH<sub>3</sub>PbI<sub>3</sub> Perovskites Predicted from First-Principles. *Sci. Rep.* **2016**, *6* (1), 19968.
- (57) Ponč, S. P.; Schlipf, M.; Giustino, F. Origin of Low Carrier Mobilities in Halide Perovskites. *ACS Energy Lett.* **2019**, *4*, 456.
- (58) Yu, H.; Zhang, Q.; Zhang, Y.; Lu, K.; Han, C.; Yang, Y.; Wang, K.; Wang, X.; Wang, M.; Zhang, J.; et al. Using Mechanical Stress to Investigate the Rashba Effect in Organic-Inorganic Hybrid Perovskites. *J. Phys. Chem. Lett.* **2019**, *10*, 5446–5450.
- (59) Kepenekian, M.; Even, J. Rashba and Dresselhaus Couplings in Halide Perovskites: Accomplishments and Opportunities for Spintronics and Spin - Orbitronics. *J. Phys. Chem. Lett.* **2017**, *8*, 3362–3370.

- (60) Haney, P.; Vardeny, Z. V.; Baniya, S.; Ehrenfreund, E.; Sheng, C.-X.; Li, J.; Zhai, Y.; Zhang, C. Giant Rashba Splitting in 2D Organic-Inorganic Halide Perovskites Measured by Transient Spectroscopies. *Sci. Adv.* **2017**, *3* (7), No. e1700704.
- (61) Zheng, F.; Tan, L. Z.; Liu, S.; Rappe, A. M. Rashba Spin-Orbit Coupling Enhanced Carrier Lifetime in CH<sub>3</sub>NH<sub>3</sub>PbI<sub>3</sub>. *Nano Lett.* **2015**, *15* (12), 7794–7800.
- (62) Etienne, T.; Mosconi, E.; De Angelis, F. Dynamical Origin of the Rashba Effect in Organohalide Lead Perovskites: A Key to Suppressed Carrier Recombination in Perovskite Solar Cells? *J. Phys. Chem. Lett.* **2016**, *7* (9), 1638–1645.
- (63) Niesner, D.; Wilhelm, M.; Levchuk, I.; Osvet, A.; Shrestha, S.; Batentschuk, M.; Brabec, C.; Fauster, T. Giant Rashba Splitting in CH<sub>3</sub>NH<sub>3</sub>PbBr<sub>3</sub> Organic-Inorganic Perovskite. *Phys. Rev. Lett.* **2016**, *117* (12), 126401.
- (64) Stranks, S. D.; Plochocka, P. The Influence of the Rashba Effect. *Nat. Mater.* **2018**, *17* (5), 381–382.
- (65) Zhou, L.; Katan, C.; Nie, W.; Tsai, H.; Pedesseau, L.; Crochet, J. J.; Even, J.; Mohite, A. D.; Tretiak, S.; Neukirch, A. J. Cation Alloying Delocalizes Polarons in Lead-Halide Perovskites. *J. Phys. Chem. Lett.* **2019**, *10* (13), 3516–3524.
- (66) Mahata, A.; Meggiolaro, D.; De Angelis, F. From Large to Small Polarons in Lead, Tin, and Mixed Lead-Tin Halide Perovskites. *J. Phys. Chem. Lett.* **2019**, *10* (8), 1790–1798.
- (67) Erhart, P.; Klein, A.; Åberg, D.; Sadigh, B. Efficacy of the DFT + U Formalism for Modeling Hole Polarons in Perovskite Oxides Efficacy of the DFT + U Formalism for ... Erhart, Klein, Åberg, and Sadigh. *Phys. Rev. B: Condens. Matter Mater. Phys.* **2014**, *90* (3), 1–8.
- (68) Cinquanta, E.; Meggiolaro, D.; Motti, S. G.; Gandini, M.; Alcocer, M. J. P.; Akkerman, Q. A.; Vozzi, C.; Manna, L.; De Angelis, F.; Petrozza, A.; et al. Ultrafast THz Probe of Photoinduced Polarons in Lead-Halide Perovskites. *Phys. Rev. Lett.* **2019**, *122* (16), 166601.
- (69) Welch, E.; Scolaro, L.; Zakhidov, A. Density Functional Theory + U Modeling of Polarons in Organohalide Lead Perovskites. *AIP Adv.* **2016**, *6* (12), 125037.
- (70) Miyata, K.; Meggiolaro, D.; Trinh, M. T.; Joshi, P. P.; Mosconi, E.; Jones, S. C.; De Angelis, F.; Zhu, X. Y. Large Polarons in Lead Halide Perovskites. *Sci. Adv.* **2017**, *3* (8), e1701217.
- (71) Kandada, A. R. S.; Silva, C. Perspective: Exciton Polarons in Two-Dimensional Hybrid Metal-Halide Perovskites. *arxiv.org* **2019**.
- (72) Johansson, M.; Lemmens, P. Crystallography and Chemistry of Perovskites. *Handb. Magn. Adv. Magn. Mater.* **2007**, *4*, 1–9.
- (73) Goldschmidt, V. M. Die Gesetze Der Krystallochemie. *Naturwissenschaften* **1926**, *14* (21), 477–485.
- (74) Gholipour, S.; Ali, A. M.; Correa-Baena, J.-P.; Turren-Cruz, S.-H.; Tajabadi, F.; Tress, W.; Taghavinia, N.; Grätzel, M.; Abate, A.; De Angelis, F.; et al. Globularity-Selected Large Molecules for a New Generation of Multication Perovskites. *Adv. Mater.* **2017**, *29* (38), 1702005.
- (75) McMeekin, D. P.; Sadoughi, G.; Rehman, W.; Eperon, G. E.; Saliba, M.; Hörlantner, M. T.; Haghighirad, A.; Sakai, N.; Korte, L.; Rech, B.; et al. A Mixed-Cation Lead Mixed-Halide Perovskite Absorber for Tandem Solar Cells. *Science* **2016**, *351* (6269), 151–155.
- (76) Ghosh, D.; Smith, A. R.; Walker, A. B.; Islam, M. S. Mixed A-Cation Perovskites for Solar Cells: Atomic-Scale Insights Into Structural Distortion, Hydrogen Bonding, and Electronic Properties. *Chem. Mater.* **2018**, *30* (15), 5194–5204.
- (77) Pering, S. R.; Deng, W.; Troughton, J. R.; Kubiak, P. S.; Ghosh, D.; Niemann, R. G.; Brivio, F.; Jeffrey, F. E.; Walker, A. B.; Islam, M. S. Azetidinium Lead Iodide for Perovskite Solar Cells. *J. Mater. Chem. A* **2017**, *5* (39), 20658.
- (78) Nagane, S.; Ghosh, D.; Hoye, R. L. Z.; Zhao, B.; Ahmad, S.; Walker, A. B.; Islam, M. S.; Ogale, S.; Sadhanala, A. Lead-Free Perovskite Semiconductors Based on Germanium-Tin Solid Solutions: Structural and Optoelectronic Properties. *J. Phys. Chem. C* **2018**, *122* (11), 5940.
- (79) Ferdani, D.; Pering, S.; Ghosh, D.; Kubiak, P.; Walker, A.; Lewis, S. E.; Johnson, A. L.; Baker, P. J.; Islam, S.; Cameron, P. J. Partial Cation Substitution Reduces Iodide Ion Transport in Lead Iodide Perovskite Solar Cells. *Energy Environ. Sci.* **2019**, *12*, 2264–2272.
- (80) Brivio, F.; Frost, J. M.; Skelton, J. M.; Jackson, A. J.; Weber, O. J.; Weller, M. T.; Goñi, A. R.; Leguy, A. M. A.; Barnes, P. R. F.; Walsh, A. Lattice Dynamics and Vibrational Spectra of the Orthorhombic, Tetragonal, and Cubic Phases of Methylammonium Lead Iodide. *Phys. Rev. B: Condens. Matter Mater. Phys.* **2015**, *92* (14), 144308 DOI: 10.1103/PhysRevB.92.144308.
- (81) Whitfield, P. S.; Herron, N.; Guise, W. E.; Page, K.; Cheng, Y. Q.; Milas, I.; Crawford, M. K. Structures, Phase Transitions and Tricritical Behavior of the Hybrid Perovskite Methyl Ammonium Lead Iodide. *Sci. Rep.* **2016**, *6*, 6.
- (82) Weber, O. J.; Ghosh, D.; Gaines, S.; Henry, P. F.; Walker, A. B.; Islam, M. S.; Weller, M. T. Phase Behavior and Polymorphism of Formamidinium Lead Iodide. *Chem. Mater.* **2018**, *30* (11), 3768–3778.
- (83) Weller, M. T.; Weber, O. J.; Henry, P. F.; Di Pumpo, M.; Hansen, T. C. Complete Structure and Cation Orientation in the Perovskite Photovoltaic Methylammonium Lead Iodide between 100 and 352 K. *Chem. Commun.* **2015**, *51*, 4180.
- (84) Motta, C.; Sanvito, S. Electron-Phonon Coupling and Polaron Mobility in Hybrid Perovskites from First Principles. *J. Phys. Chem. C* **2018**, *122* (2), 1361–1366.
- (85) Lan, Y.; Dringoli, B.; Valverde-Chavez, D.; Ponseca, C.; Sutton, M.; He, Y.; Kanatzidis, M.; Cooke, D. Ultrafast Correlated Charge and Lattice Motion in a Hybrid Metal Halide Perovskite. *Sci. Adv.* **2019**, *5* (5), eaaw5558.
- (86) Milot, R. L.; Eperon, G. E.; Snaith, H. J.; Johnston, M. B.; Herz, L. M. Temperature-Dependent Charge-Carrier Dynamics in CH<sub>3</sub>NH<sub>3</sub>PbI<sub>3</sub> Perovskite Thin Films. *Adv. Funct. Mater.* **2015**, *25* (39), 6218–6227.
- (87) Fu, J.; Xu, Q.; Han, G.; Wu, B.; Huan, C. H. A.; Leek, M. L.; Sum, T. C. Hot Carrier Cooling Mechanisms in Halide Perovskites. *Nat. Commun.* **2017**, *8* (1), 1300 DOI: 10.1038/s41467-017-01360-3.
- (88) Yang, Y.; Ostrowski, D. P.; France, R. M.; Zhu, K.; Van De Lagemaat, J.; Luther, J. M.; Beard, M. C. Observation of a Hot-Phonon Bottleneck in Lead-Iodide Perovskites. *Nat. Photonics* **2016**, *10* (1), 53–59.
- (89) Wilson, J. N.; Frost, J. M.; Wallace, S. K.; Walsh, A. Dielectric and Ferroic Properties of Metal Halide Perovskites. *APL Mater.* **2019**, *7* (1), 010901.
- (90) Karakus, M.; Jensen, S. A.; D'Angelo, F.; Turchinovich, D.; Bonn, M.; Cánovas, E. Phonon-Electron Scattering Limits Free Charge Mobility in Methylammonium Lead Iodide Perovskites. *J. Phys. Chem. Lett.* **2015**, *6* (24), 4991–4996.
- (91) Wang, Y.; Zhang, Y.; Zhang, P.; Zhang, W. High Intrinsic Carrier Mobility and Photon Absorption in the Perovskite CH<sub>3</sub>NH<sub>3</sub>PbI<sub>3</sub>. *Phys. Chem. Chem. Phys.* **2015**, *17* (17), 11516–11520.
- (92) He, Y.; Galli, G. Perovskites for Solar Thermoelectric Applications: A First Principle Study of CH<sub>3</sub>NH<sub>3</sub>AI<sub>3</sub> (A = Pb and Sn). *Chem. Mater.* **2014**, *26* (18), 5394–5400.
- (93) Fröhlich, H. Electrons in Lattice Fields. *Adv. Phys.* **1954**, *3* (11), 325–361.
- (94) Poncé, S.; Schlipf, M.; Giustino, F. Origin of Low Carrier Mobilities in Halide Perovskites. *ACS Energy Lett.* **2019**, *4* (2), 456–463.
- (95) Karakus, M.; Jensen, S. A.; D'Angelo, F.; Turchinovich, D.; Bonn, M.; Cánovas, E. C. Phonon-Electron Scattering Limits Free Charge Mobility in Methylammonium Lead Iodide Perovskites. *J. Phys. Chem. Lett.* **2015**, *6*, 4991.
- (96) Yu, P. Y.; Cardona, M. *Fundamentals of Semiconductors*; **2010**. DOI: 10.1007/978-3-642-00710-1.
- (97) Neukirch, A. J.; Nie, W.; Blancon, J. C.; Appavoo, K.; Tsai, H.; Sfeir, M. Y.; Katan, C.; Pedesseau, L.; Even, J.; Crochet, J. J.; et al. Polaron Stabilization by Cooperative Lattice Distortion and Cation Rotations in Hybrid Perovskite Materials. *Nano Lett.* **2016**, *16* (6), 3809–3816.



- (98) Even, J.; Pedesseau, L.; Katan, C. Analysis of Multivalley and Multibandgap Absorption and Enhancement of Free Carriers Related to Exciton Screening in Hybrid Perovskites. *J. Phys. Chem. C* **2014**, *118* (22), 11566–11572.
- (99) Milot, R. L.; Klug, M. T.; Davies, C. L.; Wang, Z.; Kraus, H.; Snaith, H. J.; Johnston, M. B.; Herz, L. M. The Effects of Doping Density and Temperature on the Optoelectronic Properties of Formamidinium Tin Triiodide Thin Films. *Adv. Mater.* **2018**, *30* (44), 1804506.
- (100) Sendner, M.; Nayak, P. K.; Egger, D. A.; Beck, S.; Müller, C.; Epding, B.; Kowalsky, W.; Kronik, L.; Snaith, H. J.; Pucci, A.; et al. Optical Phonons in Methylammonium Lead Halide Perovskites and Implications for Charge Transport. *Mater. Horiz.* **2016**, *3* (6), 613–620.
- (101) Cohen, R. E.; Krakauer, H. Electronic Structure Studies of the Differences in Ferroelectric Behavior of BaTiO<sub>3</sub> and PbTiO<sub>3</sub>. *Ferroelectrics* **1992**, *136* (1), 65–83.
- (102) Yang, S. Y.; Seidel, J.; Byrnes, S. J.; Shafer, P.; Yang, C. H.; Rossell, M. D.; Yu, P.; Chu, Y. H.; Scott, J. F.; Ager, J. W.; et al. Above-Bandgap Voltages from Ferroelectric Photovoltaic Devices. *Nat. Nanotechnol.* **2010**, *5* (2), 143–147.
- (103) Smith, E. H.; Benedek, N. A.; Fennie, C. J. Interplay of Octahedral Rotations and Lone Pair Ferroelectricity in CsPbF<sub>3</sub>. *Inorg. Chem.* **2015**, *54* (17), 8536–8543.
- (104) Meloni, S.; Moehl, T.; Tress, W.; Franckevius, M.; Saliba, M.; Lee, Y. H.; Gao, P.; Nazeeruddin, M. K.; Zakeeruddin, S. M.; Rothlisberger, U.; et al. Ionic Polarization-Induced Current-Voltage Hysteresis in CH<sub>3</sub>NH<sub>3</sub>PbX<sub>3</sub> perovskite Solar Cells. *Nat. Commun.* **2016**, *7*, 10334.
- (105) Frost, J. M.; Butler, K. T.; Brivio, F.; Hendon, C. H.; van Schilfgaarde, M.; Walsh, A. Atomistic Origins of High-Performance in Hybrid Halide Perovskite Solar Cells. *Nano Lett.* **2014**, *14*, 2584.
- (106) Garten, L. M.; Moore, D. T.; Nanayakkara, S. U.; Dwaraknath, S.; Schulz, P.; Wands, J.; Rockett, A.; Newell, B.; Persson, K. A.; Trolrier-McKinstry, S. The Existence and Impact of Persistent Ferroelectric Domains in MAPbI<sub>3</sub>. *Sci. Adv.* **2019**, *5* (1), eaas9311.
- (107) Hutter, E. M.; Gélvez-Rueda, M. C. M. C.; Oshero, A.; Bulović, V.; Grozema, F. C.; Stranks, S. D.; Savenije, T. J. Direct-Indirect Character of the Bandgap in Methylammonium Lead Iodide Perovskite. *Nat. Mater.* **2017**, *16* (1), 115–120.
- (108) Even, J.; Pedesseau, L.; Jancu, J.-M.; Katan, C. Importance of Spin-Orbit Coupling in Hybrid Organic/Inorganic Perovskites for Photovoltaic Applications. *J. Phys. Chem. Lett.* **2013**, *4* (17), 2999–3005.
- (109) Rashba, E. I. Symmetry of Energy Bands in Crystals of Wurtzite Type. I. Symmetry of Bands Disregarding Spin-Orbit Interaction. *Sov. Phys. Solid State* **1959**, *1* (3), 368–380.
- (110) Dresselhaus, G. Spin-Orbit Coupling Effects in Zinc Blende Structures. *Phys. Rev.* **1955**, *100* (2), 580.
- (111) Demchenko, D. O.; Izyumskaya, N.; Feneberg, M.; Avrutin, V.; Özgür, U.; Goldhahn, R.; Morkoç, H. Optical Properties of the Organic-Inorganic Hybrid Perovskite CH<sub>3</sub>NH<sub>3</sub>PbI<sub>3</sub>: Theory and Experiment. *Phys. Rev. B: Condens. Matter Mater. Phys.* **2016**, *94* (7), 075206.
- (112) Kepenekian, M.; Robles, R.; Katan, C.; Saponi, D.; Pedesseau, L.; Even, J. Rashba and Dresselhaus Effects in Hybrid Organic-Inorganic Perovskites: From Basics to Devices. *ACS Nano* **2015**, *9* (12), 11557–11567.
- (113) Umari, P.; Mosconi, E.; De Angelis, F. Relativistic GW Calculations on CH<sub>3</sub>NH<sub>3</sub>PbI<sub>3</sub> and CH<sub>3</sub>NH<sub>3</sub>SnI<sub>3</sub> Perovskites for Solar Cell Applications. *Sci. Rep.* **2015**, *4*, 4.
- (114) Giovanni, D.; Ma, H.; Chua, J.; Grätzel, M.; Ramesh, R.; Mhaisalkar, S.; Mathews, N.; Sum, T. C. Highly Spin-Polarized Carrier Dynamics and Ultralarge Photoinduced Magnetization in CH<sub>3</sub>NH<sub>3</sub>PbI<sub>3</sub> Perovskite Thin Films. *Nano Lett.* **2015**, *15* (3), 1553–1558.
- (115) Bokdam, M.; Sander, T.; Stroppa, A.; Picozzi, S.; Sarma, D. D.; Franchini, C.; Kresse, G. Role of Polar Phonons in the Photo-Excited State of Metal Halide Perovskites OPEN. *Sci. Rep.* **2016**, *6*, 28618.
- (116) Mante, P. A.; Stoumpos, C. C.; Kanatzidis, M. G.; Yartsev, A. Electron-Acoustic Phonon Coupling in Single Crystal CH<sub>3</sub>NH<sub>3</sub>PbI<sub>3</sub> Perovskites Revealed by Coherent Acoustic Phonons. *Nat. Commun.* **2017**, *8*, 1–7.
- (117) Holstein, T. Studies of Polaron Motion. Part II. The “Small” Polaron. *Ann. Phys. (Amsterdam, Neth.)* **1959**, *8* (3), 343–389.
- (118) Emin, D. *Polarons*, 1st ed.; Cambridge University Press: New York, 2013. DOI: 10.1017/CBO9781139023436.002.
- (119) Landau, L. On the Motion of Electrons in a Crystal Lattice. *Phys. Z. Sowjetunion* **1933**, *3*, 664–665.
- (120) Ortmann, F.; Bechstedt, F.; Hannewald, K. Theory of Charge Transport in Organic Crystals: Beyond Holstein’s Small-Polaron Model. *Phys. Rev. B: Condens. Matter Mater. Phys.* **2009**, *79* (23), 235206 DOI: 10.1103/PhysRevB.79.235206.
- (121) Feynman, R. P. Slow Electrons in a Polar Crystal. *Phys. Rev.* **1955**, *97* (3), 660–665.
- (122) Wolf, C.; Cho, H.; Kim, Y.-H.; Lee, T.-W. Polaronic Charge Carrier-Lattice Interactions in Lead Halide Perovskites. *ChemSusChem* **2017**, *10* (19), 3705–3711.
- (123) Firsov, Y. A. Small Polarons: Transport Phenomena. *Springer Ser. Mater. Sci.* **2007**, *103*, 63–105.
- (124) Leijnse, M.; Wegewijs, M. R.; Flensberg, K. Nonlinear Thermoelectric Properties of Molecular Junctions with Vibrational Coupling. *Phys. Rev. B: Condens. Matter Mater. Phys.* **2010**, *82* (4), 045412 DOI: 10.1103/PhysRevB.82.045412.
- (125) Hulea, I. N.; Fratini, S.; Xie, H.; Mulder, C. L.; Iossad, N. N.; Rastelli, G.; Ciuchi, S.; Morpurgo, A. F. Tunable Fröhlich Polarons in Organic Single-Crystal Transistors. *Nat. Mater.* **2006**, *5* (12), 982–986.
- (126) Kang, M.; Jung, S. W.; Shin, W. J.; Sohn, Y.; Ryu, S. H.; Kim, T. K.; Hoesch, M.; Kim, K. S. Holstein Polaron in a Valley-Degenerate Two-Dimensional Semiconductor. *Nat. Mater.* **2018**, *17* (8), 676–680.
- (127) Mott, N. Polarons in Transition-Metal Oxide. *Comments Solid State Phys.* **1968**, *1* (4), 105–111.
- (128) Podzorov, V.; Menard, E.; Borissov, A.; Kiryukhin, V.; Rogers, J. A.; Gershenson, M. E. Intrinsic Charge Transport on the Surface of Organic Semiconductors. *Phys. Rev. Lett.* **2004**, *93* (8), 086602 DOI: 10.1103/PhysRevLett.93.086602.
- (129) Zhugayevych, A.; Tretiak, S. Theoretical Description of Structural and Electronic Properties of Organic Photovoltaic Materials. *Annu. Rev. Phys. Chem.* **2015**, *66* (1), 305–330.
- (130) Mahan, G. D. *Introductory Material*. In *Many-Particle Physics*; Springer US: Boston, MA, 2000; pp 1–64. DOI: 10.1007/978-1-4757-5714-9\_1.
- (131) Alexandrov, A. S. Many-Body Effects in the Normal-State Polaron System. *Phys. Rev. B: Condens. Matter Mater. Phys.* **1992**, *46* (5), 2838–2844.
- (132) Marsiglio, F. Pairing in the Holstein Model in the Dilute Limit. *Phys. C* **1995**, *244* (1–2), 21–34.
- (133) Kubař, T.; Elstner, M.; Popescu, B.; Kleinekathöfer, U. Polaron Effects on Charge Transport through Molecular Wires: A Multiscale Approach. *J. Chem. Theory Comput.* **2017**, *13* (1), 286–296.
- (134) Jortner, J.; Bixon, M.; Langenbacher, T.; Michel-Beyerle, M. E. Charge Transfer and Transport in DNA. *Proc. Natl. Acad. Sci. U. S. A.* **1998**, *95* (22), 12759–12765.
- (135) Prodanović, N.; Vukmirović, N.; Ikonić, Z.; Harrison, P.; Indjin, D. Importance of Polaronic Effects for Charge Transport in CdSe Quantum Dot Solids. *J. Phys. Chem. Lett.* **2014**, *5* (8), 1335–1340.
- (136) Zhang, Z.; Long, R.; Tokina, M. V.; Prezhdo, O. V. Interplay between Localized and Free Charge Carriers Can Explain Hot Fluorescence in the CH<sub>3</sub>NH<sub>3</sub>PbBr<sub>3</sub> Perovskite: Time-Domain Ab Initio Analysis. *J. Am. Chem. Soc.* **2017**, *139*, 17327.

- (137) Nayyar, I. H.; Batista, E. R.; Tretiak, S.; Saxena, A.; Smith, D. L.; Martin, R. L. Localization of Electronic Excitations in Conjugated Polymers Studied by DFT. *J. Phys. Chem. Lett.* **2011**, *2* (6), 566–571.
- (138) Frost, J. M. Calculating Polaron Mobility in Halide Perovskites. *Phys. Rev. B: Condens. Matter Mater. Phys.* **2017**, *96* (19), 1–10.
- (139) Wright, A. D.; Verdi, C.; Milot, R. L.; Eperon, G. E.; Pérez-Osorio, M. A.; Snaith, H. J.; Giustino, F.; Johnston, M. B.; Herz, L. M. Electron-Phonon Coupling in Hybrid Lead Halide Perovskites. *Nat. Commun.* **2016**, *7*, 11755.
- (140) Miyata, K.; Atallah, T. L.; Zhu, X. Y. Lead Halide Perovskites: Crystal-Liquid Duality, Phonon Glass Electron Crystals, and Large Polaron Formation. *Sci. Adv.* **2017**, *3* (10), e1701469.
- (141) Neukirch, A. J.; Abate, I. I.; Zhou, L.; Nie, W.; Tsai, H.; Pedesseau, L.; Even, J.; Crochet, J. J.; Mohite, A. D.; Katan, C.; et al. Geometry Distortion and Small Polaron Binding Energy Changes with Ionic Substitution in Halide Perovskites. *J. Phys. Chem. Lett.* **2018**, *9* (24), 7130–7136.
- (142) Zheng, F.; Wang, L. Large Polaron Formation and Its Effect on Electron Transport in Hybrid Perovskites. *Energy Environ. Sci.* **2019**, *12*, 1219.
- (143) Park, M.; Neukirch, A. J.; Reyes-Lillo, S. E.; Lai, M.; Ellis, S. R.; Dietze, D.; Neaton, J. B.; Yang, P.; Tretiak, S.; Mathies, R. A. Excited-State Vibrational Dynamics toward the Polaron in Methylammonium Lead Iodide Perovskite. *Nat. Commun.* **2018**, *9* (1), 1–9.
- (144) Obratsov, P. A.; Lyashenko, D.; Chizhov, P. A.; Konishi, K.; Nemoto, N.; Kuwata-Gonokami, M.; Welch, E.; Obratsov, A. N.; Zakhidov, A. Ultrafast Zero-Bias Photocurrent and Terahertz Emission in Hybrid Perovskites. *Commun. Phys.* **2018**, *1* (14), 14 DOI: 10.1038/s42005-018-0013-8.
- (145) Gong, J.; Yang, M.; Ma, X.; Schaller, R. D.; Liu, G.; Kong, L.; Yang, Y.; Beard, M. C.; Lesslie, M.; Dai, Y.; et al. Electron–Rotor Interaction in Organic–Inorganic Lead Iodide Perovskites Discovered by Isotope Effects. *J. Phys. Chem. Lett.* **2016**, *7* (15), 2879–2887.
- (146) Zheng, K.; Abdellah, M.; Zhu, Q.; Kong, Q.; Jennings, G.; Kurtz, C.; Messing, M.; Niu, Y.; Gosztola, D.; Al-Marri, M.; et al. Direct Experimental Evidence for Photoinduced Strong-Coupling Polarons in Organolead Halide Perovskite Nanoparticles. *J. Phys. Chem. Lett.* **2016**, *7*, 4535–4539.
- (147) Brenner, T. M.; Egger, D. A.; Kronik, L.; Hodes, G.; Cahen, D. Hybrid Organic–Inorganic Perovskites: Low-Cost Semiconductors with Intriguing Charge-Transport Properties. *Nat. Rev. Mater.* **2016**, *1* (1), 15007.
- (148) Yu, Z.-G. Rashba Effect and Carrier Mobility in Hybrid Organic-Inorganic Perovskites. *J. Phys. Chem. Lett.* **2016**, *7*, 3078.
- (149) Zheng, K.; Abdellah, M.; Zhu, Q.; Kong, Q.; Jennings, G.; Kurtz, C. A.; Messing, M. E.; Niu, Y.; Gosztola, D. J.; Al-Marri, M. J.; et al. Direct Experimental Evidence for Photoinduced Strong-Coupling Polarons in Organolead Halide Perovskite Nanoparticles. *J. Phys. Chem. Lett.* **2016**, *7* (22), 4535–4539.
- (150) Thouin, F.; Valverde-Chávez, D. A.; Quarti, C.; Cortecchia, D.; Bargigia, I.; Beljonne, D.; Petrozza, A.; Silva, C.; Srimath Kandada, A. R. Phonon Coherences Reveal the Polaronic Character of Excitons in Two-Dimensional Lead Halide Perovskites. *Nat. Mater.* **2019**, *18* (4), 349–356.
- (151) Yanai, T.; Tew, D. P.; Handy, N. C. A New Hybrid Exchange-Correlation Functional Using the Coulomb-Attenuating Method (CAM-B3LYP). *Chem. Phys. Lett.* **2004**, *393* (1–3), 51–57.
- (152) Gualdrón-Reyes, A. F.; Yoon, S. J.; Mora-Seró, I. Recent Insights for Achieving Mixed Halide Perovskites without Halide Segregation. *Curr. Opin. Electrochem.* **2018**, *11*, 84–90.
- (153) Diab, H.; Trippé-Allard, G.; Lédée, F.; Jemli, K.; Vilar, C.; Bouchez, G.; Jacques, V. L. R.; Tejeda, A.; Even, J.; Lauret, J. S.; et al. Narrow Linewidth Excitonic Emission in Organic-Inorganic Lead Iodide Perovskite Single Crystals. *J. Phys. Chem. Lett.* **2016**, *7* (24), 5093–5100.
- (154) Soufiani, A. M.; Huang, F.; Reece, P.; Sheng, R.; Ho-Baillie, A.; Green, M. A. Polaronic Exciton Binding Energy in Iodide and Bromide Organic-Inorganic Lead Halide Perovskites. *Appl. Phys. Lett.* **2015**, *107* (23), 231902.
- (155) Tsai, H.; Asadpour, R.; Blancon, J.-C.; Stoumpos, C. C.; Durand, O.; Strzalka, J. W.; Chen, B.; Verduzco, R.; Ajayan, P. M.; Tretiak, S.; et al. Light-Induced Lattice Expansion Leads to High-Efficiency Perovskite Solar Cells. *Science (Washington, DC, U. S.)* **2018**, *360* (6384), 67–70.
- (156) Singh, T.; Miyasaka, T. Stabilizing the Efficiency beyond 20% with a Mixed Cation Perovskite Solar Cell Fabricated in Ambient Air under Controlled Humidity. *Adv. Funct. Mater.* **2018**, *8* (3), 1700677.
- (157) Kim, H.-S.; Hagfeldt, A. Photoinduced Lattice Symmetry Enhancement in Mixed Hybrid Perovskites and Its Beneficial Effect on the Recombination Behavior. *Adv. Opt. Mater.* **2019**, *7*, 1801512.
- (158) Pellet, N.; Gao, P.; Gregori, G.; Yang, T. Y.; Nazeeruddin, M. K.; Maier, J.; Grätzel, M. Mixed-Organic-Cation Perovskite Photovoltaics for Enhanced Solar-Light Harvesting. *Angew. Chem., Int. Ed.* **2014**, *53*, 3151.
- (159) Wang, Z.; McMeekin, D. P.; Sakai, N.; van Reenen, S.; Wojciechowski, K.; Patel, J. B.; Johnston, M. B.; Snaith, H. J. Efficient and Air-Stable Mixed-Cation Lead Mixed-Halide Perovskite Solar Cells with n-Doped Organic Electron Extraction Layers. *Adv. Mater.* **2017**, *29* (5), 1604186.
- (160) Rehman, W.; McMeekin, D. P.; Patel, J. B.; Milot, R. L.; Johnston, M. B.; Snaith, H. J.; Herz, L. M. Photovoltaic Mixed-Cation Lead Mixed-Halide Perovskites: Links between Crystallinity, Photo-Stability and Electronic Properties. *Energy Environ. Sci.* **2017**, *10*, 361–369.
- (161) Brenner, T. M.; Egger, D. A.; Rappe, A. M.; Kronik, L.; Hodes, G.; Cahen, D. Are Mobilities in Hybrid Organic-Inorganic Halide Perovskites Actually “High”? *J. Phys. Chem. Lett.* **2015**, *6* (23), 4754–4757.
- (162) Frost, J. M.; Walsh, A. What Is Moving in Hybrid Halide Perovskite Solar Cells? *Acc. Chem. Res.* **2016**, *49*, 528–535, DOI: 10.1021/acs.accounts.5b00431.
- (163) Zhang, M.; Zhang, X.; Huang, L. Y.; Lin, H. Q.; Lu, G. Charge Transport in Hybrid Halide Perovskites. *Phys. Rev. B: Condens. Matter Mater. Phys.* **2017**, *96* (19), 1–7.
- (164) Yin, J.; Maity, P.; De Bastiani, M.; Dursun, I.; Bakr, O. M.; Brédas, J. L.; Mohammed, O. F. Molecular Behavior of Zero-Dimensional Perovskites. *Sci. Adv.* **2017**, *3* (12), e1701793.
- (165) Zhu, H.; Miyata, K.; Fu, Y.; Wang, J.; Joshi, P. P.; Niesner, D.; Williams, K. W.; Jin, S.; Zhu, X. Y. Screening in Crystalline Liquids Protects Energetic Carriers in Hybrid Perovskites. *Science (Washington, DC, U. S.)* **2016**, *353* (6306), 1409–1413.
- (166) Zhu, X. Y.; Podzorov, V. Charge Carriers in Hybrid Organic-Inorganic Lead Halide Perovskites Might Be Protected as Large Polarons. *J. Phys. Chem. Lett.* **2015**, *6* (23), 4758–4761.
- (167) Frost, J. M.; Whalley, L. D.; Walsh, A. Slow Cooling of Hot Polarons in Halide Perovskite Solar Cells. *ACS Energy Lett.* **2017**, *2* (12), 2647–2652.
- (168) Emin, D. Barrier to Recombination of Oppositely Charged Large Polarons. *J. Appl. Phys.* **2018**, *123* (5), 055105.
- (169) Guo, Z.; Wan, Y.; Yang, M.; Snaider, J.; Zhu, K.; Huang, L. Long-Range Hot-Carrier Transport in Hybrid Perovskites Visualized by Ultrafast Microscopy. *Science (Washington, DC, U. S.)* **2017**, *356* (6333), 59–62.
- (170) Price, M. B.; Butkus, J.; Jellicoe, T. C.; Sadhanala, A.; Briane, A.; Halpert, J. E.; Broch, K.; Hodgkiss, J. M.; Friend, R. H.; Deschler, F. Hot-Carrier Cooling and Photoinduced Refractive Index Changes in Organic-Inorganic Lead Halide Perovskites. *Nat. Commun.* **2015**, *6* (May), 1–8.
- (171) Niesner, D.; Zhu, H.; Miyata, K.; Joshi, P. P.; Evans, T. J. S.; Kudisch, B. J.; Trinh, M. T.; Marks, M.; Zhu, X. Y. Persistent Energetic Electrons in Methylammonium Lead Iodide Perovskite Thin Films. *J. Am. Chem. Soc.* **2016**, *138* (48), 15717–15726.